Final Report: Exploration of Platform-Level Impacts of Flywheel Energy Storage

N00014-18-1-2656

Matthew Collette [1], **Stein Housner, Joseph van Houten, Peter Rohrer, Nate Clemett, Ben Simmons**

MSDL Report Number: 2022-002

Date: November 11 2022

Abstract: Flywheel energy storage devices (FESD) have been proposed for a range of naval vessels. However, their broader impact on ship design has not been quantified. This report explores the design impact of such systems, looking at conventional design parameters such as space and weight alongside the impact of the forces generated by the FESD on the vessel. For a frigate-sized vessel, the impacts are generally small and dominated by changes in weight. Smaller vessels with long low-power periods in their operational profile can also benefit from FESD, where the impacts are generally larger. The potential to use the gyroscopic forces produced by FESD is explored with both modifications to a linear strip theory code and a scale model test of a modern tumblehome hullform. Both passive and active stabilization approaches are shown to be highly effective and could result in the removal of fin stabilizers from boats fitted with FESD. However, the active control forces needed may require more than one FESD to be configured to act as a stabilizer depending on the vessel's size. Through the course of this work, eight students were trained in the issues around energy storage, autonomy, ship motions, and ship design.

Marine Structures Design Lab
Department of Naval Architecture and Marine Engineering
University of Michigan, 2600 Draper Drive
Ann Arbor, Michigan 48109
msdl.engin.umich.edu

[1]Corresponding Author, University of Michigan NA&ME Department, mdcoll@umich.edu

Contents

1 Student Participation

A major focus of this project was to develop and train a large number of students in the interaction between energy systems and marine design. The major contributors to this project are listed below, though many other student interns at the Marine Hydrodynamics Lab helped on test days and in other smaller roles. Five of the students worked on the projects as undergraduates, and of those, two continued to work on the project as graduate students. From the project, students have gone onto jobs directly in the Navy (NSWCCCD-Combatant Craft) or in related energy fields (Two are NREL doing offshore energy, and a further two are doing PhDs at other institutions focused on offshore energy)

Table 1: Student Roles throughout the Project

Student	**Role**	**Timeframe**
Joseph van Houten:	Impact on ship motions thesis, AMTS paper	W2018 - S2019
Peter Rohrer:	Small vessel and frigate energy study, AMTS paper	F2018 - S2020
Ericka Lozon:	AMTS Paper	F2018 - S2020
Matthew Pienta:	AMTS Paper	F2018 - S2020
Stein Housner:	Continuation of impact on ship motions thesis	W2018 - W2020
Raza Ali:	FESD containment and preliminary design	S2020 - W2021
Ben Simmons:	FESD design, construction, and experimentation	F2020 - F2022
Nate Clemett:	FESD design, construction, and experimentation	F2021 - F2022

2 Introduction

The U.S. Navy is currently in the midst of an electrical power transition. Concepts such as integrated electric drive, medium-voltage DC distribution systems, power electronics, directed-energy weapons, and electromagnetic launch of aircraft have moved the electrical generation and distribution system from an essential auxiliary system to a central design driver and determinant of the platform capability. This rapid transition has been marked by the emergence of many competing concepts for electrical power generation and distribution systems. Pulsed loads from railguns, lasers, and other directed energy systems, as well as the demand for backup power sources to primary generators, have led to rapid advances in energy storage technologies. Kinetic energy storage through rotating mass flywheels has been proposed for both pulse load and uninterruptible power supply applications [11]. However, flywheels have many unique features and can impact platform performance beyond energy storage.

Flywheels store energy via rotating mass, unlike charge or chemical energy storage devices such as capacitors or batteries. The use of mass to store energy presents challenges for integrating flywheel energy storage devices (FESD) into platform design. The physical configuration and space demands may be less flexible than batteries, as the mass must be concentrated together. Additionally, large physical forces result from attempting to accelerate the FESD. Such forces can be used intentionally to control vessel motion but may also cause problems in off-design conditions. At the current time, a lack of understanding of these platform-level impacts prevents exploring FESD-based design concepts with sufficient confidence to trade FESD-based storage concepts against alternative energy architectures.

Given the unique platform-level design impact of FESD, it is essential to quantify these impacts when considering energy-storage options for future naval platforms. This work reports on an initial investigation to quantify these impacts on naval platforms of different sizes, summarize these findings in a knowledge structure, and identify areas for further research. Additionally, through a series of work-study positions and internships, an experimental flywheel demonstrator was constructed for a naval vessel and tested at the University of Michigan's Marine Hydrodynamics Laboratory. The sections of this report roughly follow the progression of the project, starting with background studies on FESD themselves, then progressing through an initial study on a Frigate-sized vessel, an application for energy storage on a MUSV-sized vessel, and then a detailed exploration of motions impacts on flywheels and flywheels ability to impact ship motions.

3 Background on Flywheels

FESD can create moments through two primary means, their charge-discharge cycles and the gyroscopic effect of the spinning mass as either the ship moves or the FESD is intentionally moved by a control system. Each of these will be explored in turn.

3.1 Energy Storage

3.1.1 Energy Storage Capacity

FESD's primary purpose is to store energy. Typically, a FESD consists of a large rotating mass connected to a motor/generator. To charge the FESD, the motor/generated is used as a motor to accelerate the flywheel to high speed. When energy is desired to be removed from the system, the motor/generator becomes a generator and removes the energy from the rotating mass. For a flywheel with a mass moment of inertia, I_{rotor} and a spin velocity p, the stored energy, E, is given by:

$$E = \frac{1}{2} I p^2 \tag{1}$$

The performance of such a system is largely governed by mechanical considerations, the flywheel needs to be made from a dense but strong material that can rotate at a high speed without failing. Increasing the spin speed, p, is more efficient than increasing the moment of inertia. However, the maximum spin speed is limited owing to the hoop stress inside the flywheel owing to its rotational motion. The hoop stress, at any radius, r, for a material with density ρ for a solid flywheel can be found as:

$$\sigma_{hoop} = \rho r^2 p^2 \tag{2}$$

3.1.2 Energy Storage Moments

A common question when dealing with flywheels is what is the impact of charging and discharging the flywheel on the vessel. In general, FESD may be fitting in multiples (e.g., 8 or 12 individual FESD coupled together), and by alternating the spin direction, any charging or discharging moments would cancel out. However, for smaller vessels, or in the case of a single flywheel, it is useful to look at what moment would be created during the charge-discharge cycle. In general, charging and discharging of the flywheel are achieved by applying an angular acceleration to the spinning mass. Ignoring the dynamics of the motor/generator (which may prove to be more limiting in practice than the mass alone), the torque required is given as a function of the angular acceleration, α, or the rate of change of p:

$$\tau = I\dot{p} \tag{3}$$

Suppose the assumption is made that the rate of acceleration is constant over the charge/discharge interval. In that case, the following expression emerges, using a final and initial time and spin velocity with the subscripts f and i:

$$\dot{p} = \frac{\Delta p}{\Delta t} = \frac{p_f - p_i}{t_f - t_i} \tag{4}$$

To make the formula more useful, we can express $\dot{p}$ in terms of the energy discharged (assuming ideal energy conversion):

$$\Delta E = \frac{1}{2} I(p_f^2 - p_i^2) \tag{5}$$

This can be re-arranged to yield:

$$p_f = \sqrt{\frac{2\Delta E}{I} + (p_i)^2} \tag{6}$$

Plugging this back into the acceleration equation yields:

$$\dot{p} = \frac{\sqrt{\frac{2\Delta E}{I} + (p_i)^2} - p_i}{t_f - t_i} \tag{7}$$

An example calculation can be made to show the magnitude of the flywheel forces generated. Consider a flywheel with a mass moment of inertia, I, of $400 kgm^2$, spinning at $1500 \frac{rad}{sec}$ (roughly 14,300 RPM). At this speed, the total stored energy is 450 MJ. If there is a desire to take $150 MJ$ of power out, the average de-acceleration will be:

$$\dot{p} = \frac{\sqrt{\frac{2150 MJ}{400 kgm^2} + (1500 \frac{rad}{sec})^2} - (1500 \frac{rad}{sec})^2}{6 sec - 0 sec} = -45.9 \frac{rad}{sec^2} \tag{8}$$

The flywheel will settle at a final RPM of roughly 11700 RPM, yet as the system's rotational speed is quite high, the generated torque is fairly low:

$$\tau = (400 kgm^2)(-45.9 \frac{rad}{sec^2}) = 18.35 kNm \tag{9}$$

Looking at a fairly generic smaller warship, with a length of roughly $120m$, a displacement of $4000mt$ with an upright GM of $1m$ and a moment to change trim 1 cm of $400 \frac{mt*m}{cm}$, the impact of the torque generated by the charge and discharge cycles of the flywheel is very small:

- If the flywheel is oriented with its spin axis vertical, the resulting moment will be in yaw. Assuming the rudder is roughly $60m$ aft of the pivot point in yaw, the force on the rudder to counteract the yaw moment is significantly less than $1kN$, which can easily be generated at very small rudder angles.
- If the flywheel is oriented with the spin axis running port-starboard, the resulting moment will be in pitch. However, the change in static trim will be small, far less than $1cm$ for any reasonable value of moment to change trim 1cm for this type of vessel.
- If the flywheel is oriented with the spin axis running fore-aft, the resulting torque will cause a heel response on the vessel. However, the magnitude of this response will be less than $0.1deg$.

This example did not include any considerations of the generator needed to remove the $150MJ$ over 6 seconds. Indeed, most flywheels proposed to date may struggle to generate this much power per device. The primary driving factor of this response is the relatively high RPM of modern flywheels, which reduces the torque generated significantly. A $100\frac{rad}{sec}$ flywheel (roughly 1000 RPM) would require a mass moment of inertia of $9000kgm^2$ to store the same amount of energy as the FESD above and would produce a torque of $275kNm$, almost 15 times the force generated by the higher RPM flywheel if $150MJ$ of energy was removed over 6 seconds. Likewise, deeper discharges (e.g. using more the 1/3 of the energy of the flywheel) would result in much greater angular accelerations and forces. Doubling the energy discharge to $300MJ$ (again ignoring the ability to remove this much energy in this short time window) results in the torque growing to $42.3knM$ for the $1500\frac{rad}{sec}$ FESD, more than double that of the $150MJ$ discharge. Thus, for modern, high-RPM flywheels, it is likely that the charge/discharge moments are going to have small impacts on the ship's position in the water. Overall, this conclusion is in line with existing vessels. Single-screw naval vessels may have 20-30 MW on a single shaft, rotating at much lower RPMs ($<$ 1000 RPM) with larger torques. While some small heel is noticeable at full power on these vessels, these larger moments are not considered harmful.

3.2 Gyroscopic Forces

While charge/discharge forces are likely to be small, rotating masses can generate larger gyroscopic forces. Efforts to stabilize ships with rotating masses stretch back more than 100 years at this point, though previous efforts suffered from low available spin velocities, which necessitated large rotating masses. With the much higher spin rates of FESD, it is important to explore the impact of gyroscopic forces.

3.2.1 Introduction to Gyroscopic Motion

Figure 1 shows a picture of a wheel with a moment of inertia that can rotate around its center axle, which is in the r-direction, with a spin velocity of p. The wheel hangs from the ceiling by a rope, which is in the k-direction but attaches to the wheel assembly at the end of its center axle at a distance b away from the center of gravity of the wheel. This example is commonly shown in classrooms as a bike tire hanging from the ceiling[13].

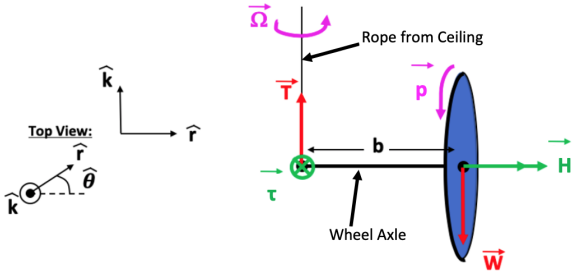

Figure 1: Bike Tire Assembly hanging from the ceiling by a rope [25]

There are two important aspects of physics that contribute to the overall gyroscopic motion of this setup. First, the force offset between the weight of the wheel and the tension in the

rope creates a torque that points into the page, which is the cross product of the righting arm b and the tension T or weight W force (both forces work with the right-hand rule to produce a torque pointing into the page τ). If the wheel is not spinning about its axle, the wheel would simply fall and pivot about the connection point of the rope and the axle until the weight and tension forces align. Secondly, in the case where the wheel is positioned how it is in Figure 1 and is spinning with a rotational velocity p in the counterclockwise direction when looking from the outside, the angular momentum of the wheel H points in the positive r-direction, using the right-hand rule.

When the wheel spins at a high enough rotational velocity and is supported only by the rope, the law of conservation of momentum causes the wheel to precess about the k-direction axis (rope axis) at velocity Ω [13].

This is gyroscopic motion. An important part of gyroscopic motion is determining the direction of precession and the precession rate. The direction of precession rotation can be physically understood in two ways. Mathematically, it can be understood as the cross-product of the angular momentum and the torque. The resultant vector points in the positive k-direction, and the wheel will precess counter-clockwise around the k-direction axis when viewed from above (using the right-hand rule) and Equation (10) shows this relationship.

$$PrecessionDirection(\Omega) = H \times \tau \tag{10}$$

Conceptually, the torque vector points into the page, and the angular momentum points in the r-direction. It can be thought that while the wheel is spinning, the torque is pulling the wheel into the page or that the angular momentum vector is "chasing" the torque vector counter-clockwise around the k-direction axis or precession axis.

3.2.2 Math and Physics

To start explaining gyroscopic motion in more mathematical terms, linear momentum will be reviewed and then correlated to angular momentum. Figure 2(a) shows a particle moving in the z-direction with speed v, which means that its linear momentum G, where $G = mv$, is also in the z-direction.

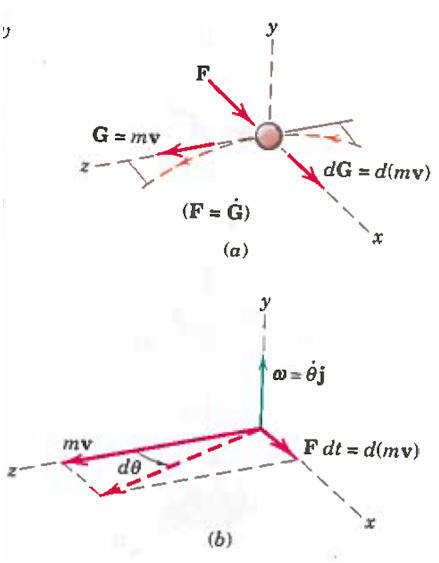

Figure 2: Pictoral analysis of Linear Momentum Physics where (a) shows the linear momentum of a particle and (b) shows the change in linear momentum [15]

A force F is applied to the particle in the x-direction, which causes a change in the particle's linear momentum dG, where $dG = d(mv)$, which also points in the x-direction. Because $F = ma = m(dv)$, F is equal to the time derivative of the linear momentum G. It can be rewritten that $Fdt = dG$ and in Figure 2(b), for small angle approximations, $tan(d\theta)$ becomes $d\theta$, where $d\theta = dG/G = Fdt/mv$. Moving the dt to the left side, $\frac{d\theta}{dt}$ is the velocity of θ, or $\dot{\theta}$, and so $F = mv\dot{\theta}$. When the angular velocity $\omega = \dot{\theta}$, Equation (11) can be written.

$$F = m\omega \times v \tag{11}$$

This means that the force on the particle is the cross-product between the mass times the angular velocity and the linear velocity of the particle.

This same concept can be applied to angular momentum. Figure 3 and Figure 4 show a rotor, which can be considered as a flywheel, that has a moment of inertia I, rotational velocity p, and is fixed about the origin of the axes.

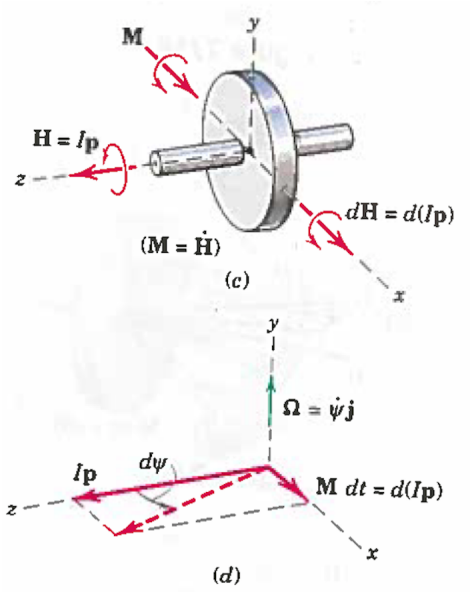

Figure 3: Pictoral Analysis of Angular Momentum [15]

The gyroscopic moment of a flywheel can be related to the spin angular velocity p of the flywheel and the precession angular velocity Ω, similarly to the variables used in Equation (11). In these figures, the flywheel has a high rate of spin p in the z-axis (Figure 3) or the spin axis (Figure 4), and a low precession rate Ω along the y-axis (Figure 3) or the precession axis (Figure 4). The spin rate creates an angular momentum H where $H = Ip$ that points along the z-axis (Figure 3). The external forces F, shown in Figure 4, applied on the flywheel's axle create an external moment on the flywheel that points along the x-axis (Figure 3), or the torque axis (Figure 4). It should be noted that the precession rate Ω is NOT caused by these two forces and is precessing due to another cause that will be explained later.

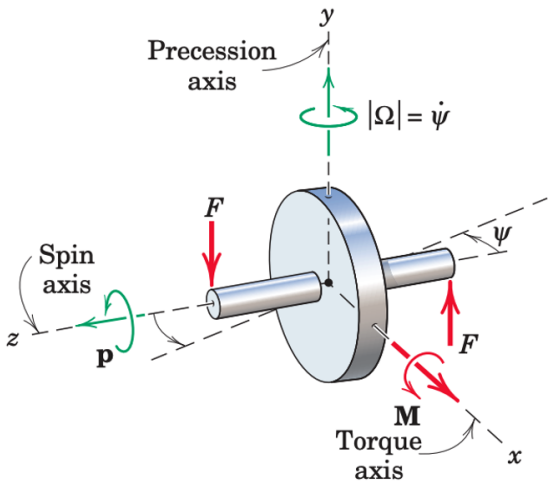

Figure 4: Rotor Diagram showing the spin axis, torque axis, and precession axis [15]

This external moment is analogous to the force applied to the particle in Figure 2 and is also

analogous to the torque created in the wheel example by the offset of the tension and weight forces. Equation (10) also justifies the precession velocity rotating in the direction shown in Figure 4, which points in positive precession axis and rotates counter-clockwise with velocity Ω when viewing from above.

Using the principles introduced in the linear momentum example, the external moment M causes a change in the wheel's angular momentum dH, where $dH = d(Ip)$, and dH also points in the positive x-direction, as seen in Figure 3(d). Because Newton's Second Law says $M = I\dot{p}$, where $\dot{p}$ is the spin acceleration ($\dot{p} = dp$), M is equal to the time derivative of the angular momentum H. It can be written that $Mdt = dH$ and in Figure 3(d), for small angle approximations, $tan(d\psi)$ becomes $d\psi$ where $d\psi = dH/H = Mdt/Ip$. Moving the dt to the left side, $\frac{d\psi}{dt}$ is the velocity of ψ ($\dot{\psi}$), and so $M = Ip\frac{d\psi}{dt} = Ip\dot{\psi}$. When $\dot{\psi} = \Omega$, then $M = Ip\Omega$, and can be represented as Equation (12) using vectors.

$$M = I\Omega \times p \tag{12}$$

This means that the induced moment from a flywheel M_{fly} is the cross product of the precession velocity Ω and the spin velocity p, which points in the same direction as the external moment. This equation governs both force and free precession, which in turn covers much of the flywheel integration on the vessel.

4 Initial Frigate Study

To look at the wider design impacts of FESD on ship designs, a FESD energy storage system was developed from previously published concepts, and the impact on a published ship design was investigated. This case study first examined the likely FESD as well as the use cases for a FESD on a frigate-sized vessel. Then a slightly revised frigate design was proposed, and the different FESD systems were investigated for this hull.

4.1 Flywheel Energy Storage Device

The FESD used for the purposes of this section was developed at the University of Texas at Austin Center for Electromechanics (UT-CEM) in 2003 and is referred to as the ALPS Flywheel (depicted in Figure 5).

Table 2: ALPS Flywheel specifications [24]

Parameter	**Value**
Rated Power	2 MW
Deliverable Energy	360 MJ
Rotor Diameter	1.32 m
Rotor Mass	2300 kg
Rotor Moment of Inertia	$389\,\mathrm{kg} * \mathrm{m}^2$
Rotor Velocity	7000 - 15000 RPM
Overall Mass	18 t
Overall Volume	$20\,\mathrm{m}^3$
Overall Deck Area	$2.5\,\mathrm{m}^2$

The ALPS Flywheel was designed for use in high-speed rail locomotives and was chosen for its very high energy storage capacity and vehicular design use case. The device consists of a composite rotor mounted on magnetic bearings in an evacuated enclosure with a motor/generator unit affixed to the outside of the enclosure. Approximate specifications of the device are included in Table 2.

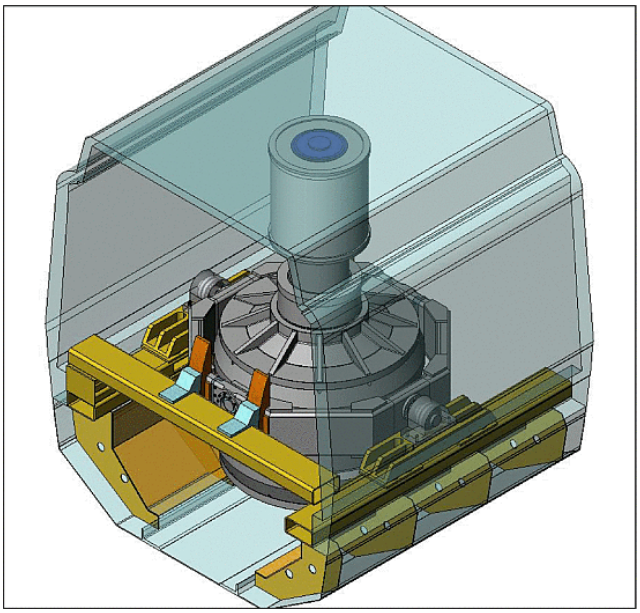

Figure 5: Illustration of the ALPS Flywheel and motor/generator unit in a locomotive mounting frame [24]

4.2 Uses for FESD Aboard Ships

Integration of a FESD into the electric grid of a ship poses great benefits with relatively low system redesign required. Integration requires a power electronic converter, a motor/generator, and a variable frequency drive to connect the flywheel to the system. This setup would allow the flywheel to run in parallel with the main generators and be used to support a large load. Given that the flywheel does not require much outfitting to be connected to the grid

means that adding flywheels in large numbers is a realistic goal.

There are many areas of application for the energy stored by flywheels, including the electric start of a vessel. The most common method to bring gas turbine engines online for naval ships is to use a compressed air system to push air through the engines. The electric start system (ESS) would allow for the removal of this pneumatic system which is more complex than the ESS. Current electric start systems have been developed and are significantly cheaper, smaller, and of less weight than the hydraulic or pneumatic systems. The current systems in use have the capability to spin the engines at varying speeds, giving them the ability to start, purge, wash, or borescope the engines [14]. Flywheels can provide the needed electricity for these electric start systems and further allow the navy to develop smarter ships.

Another promising potential use of flywheels is to allow single generator operation of naval ships. Currently, naval ships operate two generators at half load to avoid a dark ship (complete loss of electrical power). While this method maintains the reliability of the electric grid, it doubles the usage hours of both generators and decreases their efficiency. With a flywheel energy storage system, the electrical base of the ship could be supported for enough time for the second generator to come online. This setup would allow ships to operate a single generator at full load. In Hebner, Herst, and Gattozzi's 2010 paper, the fuel and cost savings of operating a single generator at full load for the Arleigh Burke class destroyers is studied [10]. Based on a ship service power of 2525 kW and 4000 operating hours, it is determined that running a single generator at full load would save $1.25 million per ship per year.

4.3 Load Case Development

To analyze the impacts of FESDs, several load cases are developed describing possible discharge scenarios. These load cases (laid out in Table 3) are created based on different electrical requirements that a FESD (or several) could be used to meet. Load cases A1 and A2 are based on short-duration, high-intensity, pulsed loads, spread over an unknown quantity for an unknown duration. Load case B is based on a single, large load over a long period of time. Load case C is based on a large, periodic load with a frequency greater than a conventional generator cycle.

Table 3: Load cases developed to explore FESD applications

Load Case	Magnitude	Duration	Power
A1	5000 MJ	10 s per 100 MJ	10 MW
A2	7500 MJ	6 s per 150 MJ	25 MW
B	4500 MJ	30 min	2.5 MW
C	30 MJ	1 min	0.5 MW

4.4 Development of the USS Ann Arbor

In order to study the platform-level impacts of flywheels on a naval vessel, a ship had to be created. The inspiration for this vessel comes from *A comparative study of US and UK frigate design* by Larrie D Ferreiro and Mark H Stonehouse [5]. This section studied US and UK

baseline frigate design for a common payload. Ferreiro and Stonehouse identified manning, propulsion, and protection as the key differences between US and UK frigate design. They developed the US Variant, which encompasses the US baseline design with UK protection, manning, and propulsion. Table 4 shows the principal characteristics of the US Variant. The US Variant is equipped with two 18 000 kW gas turbines and two 4850 kW diesel engines.

Table 4: US Variant principal characteristics [5]

Parameter	**Value**
LBP	133 m
Beam	16.1 m
Depth	9.5 m
Draft	5.1 m
LS Weight	4740 t
FL Displ	5578 t
Arrg Area	4640 m^2
Hull Volume	214 462 m^3
Deck House Volume	4210 m^3
Total Volume	18 672 m^3

To allow for more robust modeling, a hull form based on the US Variant is created in Rhinoceros 3D. This hull form (particulars in Table 5) is referred to as the USS Ann Arbor and closely matches the US Variant.

Table 5: USS Ann Arbor principal characteristics

Parameter	**Value**
LBP	133.09 m
Beam	16.1 m
Depth	9.5 m
Draft	5.1 m
Displacement	5261 t
C_B	0.555
C_M	0.758
C_{WP}	0.876
LCB	67.38 m fwd AP

4.5 Results

The results of the first-year bench study have yielded a far greater understanding of flywheel-ship interactions. They have shown that for a ship the size of the USS Ann Arbor (5261 tonnes), the impacts of FESDs are noticeable, yet not of a magnitude that would require a brand-new design or design approach.

4.5.1 Space and Weight

FESDs are significantly-sized machinery. As highlighted in Table 2, the ALPS Flywheel has a mass of 18 t and volume of 20 m^3. While a single flywheel of this size is unlikely to necessitate redesign in most medium to large naval vessels, equipping vessels with banks of several FESDs will begin to impact the design. In Table 6, the number of ALPS Flywheels required to meet the energy requirement of all four load cases are presented, along with the resulting volume, deck area, and mass estimates for the installed FESDs. Table 7 shows the calculated increase in weight of the ship and percent of arrangeable area occupied by FESDs. The percentage of the area used is taken from the total arrangeable area of the US Variant, and it is assumed to be equal to the USS Ann Arbor's arrangeable area.

Table 6: Total space and weight of FESDs for each load case

Load Case	**Flywheels Needed**	**Volume** (m^3)	**Direct Deck Area** (m^2)	**Mass** (t)
A1	14	280	35	252
A2	21	420	52.5	378
B	16	320	40	288
C	1	20	2.5	18

Table 7: Impacts on space and weight of USS Ann Arbor

Load Case	**Weight Increase**	**Arrangeable Area Increase**
A1	4.52%	0.75%
A2	6.78%	1.13%
B	5.16%	0.86%
C	0.32%	0.05%

As Table 6 and Table 7 seemingly show, the largest increases in weight and arrangeable area required corresponds with load cases involving the most flywheels. A mere 0.32% increase in weight and 0.05% increase in arrangeable area for the case of a single flywheel is negligible, but 6.78% and 1.13% increases for the case of 21 flywheels becomes significant. Note also that the area impacts only examine the flywheels themselves - most other machines on vessels typically require a total deck area of 200%-300% for access and maintenance. However, this still represents less than 4% of the arrangeable area of the vessel. Additionally, in discussions with ONR, even higher RPM flywheels are in development which would further reduce the area and weight required. For this case, engineers must take total flywheel weight and area into consideration when incorporating them into a new or existing vessel, but they should not become the main design drivers.

Despite the results from the tables accounting for precise ALPS flywheel weight and volume, they do not account for additional components paired with the flywheels that would also affect weight and space. As with all machinery installed aboard vessels, it is important to leave access for maintenance paths and potential replacement. Because of this need, it is likely that FESDs would actually require more arrangeable area than calculated in Table 6 and

be more limited in potential placement aboard a vessel. Additionally, support infrastructure that may include high-voltage cabling and power electronics, cooling equipment, and control hardware will be needed in addition to the actual devices. If the setup of a FESD allowed for modularizing or sharing this infrastructure among an array of devices, though, the total amount required would be reduced.

Lastly, the orientation and shape of a FESD greatly impacts its ability to be arranged for minimum space in a vessel. The preferred orientation for commercially available systems is to align the spin-axis with the global vertical axis, allowing for better control of moments with flywheel precession and alleviating potential sagging stress on a horizontal shaft. The shortcoming of a vertical arrangement is that the height requirement of the FESD may exceed the standard deck height used in design, necessitating a compartment over two decks.

4.5.2 Powering

To assess the impact of FESDs on vessel powering, the University of Michigan Powering Prediction Program (PPP) developed by M.G. Parsons is utilized. This program uses Holtrop and Mennen's method to estimate the resistance and hull-propeller interaction for a displacement hull. The range of applicability of the program is shown in Table 8. The values of the USS Ann Arbor fit well within the restrictions of the PPP code, validating the findings.

Table 8: PPP range of applicability

Parameters	**USS Ann Arbor Values**
$0.55 \leq C_p \leq 0.85$	0.73
$3.90 \leq \frac{L}{B} \leq 14.9$	8.27
$2.10 \leq \frac{B}{T} \leq 4.00$	3.16
$0.05 \leq F_n \leq 1.00$	0.20 - 0.40

The results of the program for the USS Ann Arbor are shown in Table 9. For each load case, the resistance is calculated at a speed of 20 knots. The greatest increase in resistance is almost 5% for the A2 load case, presumably because more flywheels lead to more weight and more drag. A 5% increase in resistance will lead to subsequent increases in effective power, brake power, engine size, and vessel cost. However, these increases can all add up quickly; once again, it should not warrant a total redesign of a vessel. The 0.43% increase in resistance from a single flywheel should be rather negligible, but not as much as the 0.32% and 0.05% increases in weight and arrangeable area, as discussed in the previous section.

Table 9: Resistance estimates of the USS Ann Arbor for each load case

Load Case	**Resistance** (kN)	**Percent Increase**
No Flywheel	519.9	-
A1	537.2	3.33%
A2	545.5	4.93%
B	540.5	3.97%
C	522.1	0.43%

5 Small Vessel Study

The initial studies of charging and discharging a flywheel and examining the flywheel's impact on a frigate-sized vessel showed relatively small impacts on the vessel design. However, there may be uses for flywheels on smaller vessels, especially unmanned vessels, where continuously using a diesel generator to produce power may result in reliability problems. This concern led to the selection of the Navy's MUSV concept as a focus for this study. Though no designs have been publically released for the concept, it is likely to fall in the range of 200 t to 500 t displacement, significantly smaller than a frigate-type vessel. The vessel will primarily be used for ISR work, and hence a quiet and highly reliable power source for loitering and observing components of the missions may be advantageous. Additionally, the small size and low forward speed of the vessel makes it more suitable for gyroscopic motion stabilization.
The purpose of this section is to explore the design impacts of incorporating FESDs on a future unmanned vessel. The specifications of the unmanned vessel are based on the US Navy RFP for a Medium Unmanned Surface Vessel (MUSV)[6]. This model exploration utilized OpenMDAO's DOEDriver and the NSGA2 optimizer (from `pyOptSparse`) for design space exploration and multivariable optimization.

5.1 Basic Model Setup

The flow of the model is largely linear, as shown in Figure 6. Several estimation methods (written as Python scripts and wrapped using the `ExplicitComponent` class) are combined to determine the weight, powering, and stability of the vessel based on the input parameters.

The model is based on a fuel estimation script. This script begins with the input variables generated in the design space exploration. Using empirical fits based on roughly similar vessels from Grubisic 2012 [8], further design characteristics are extrapolated. This vessel information is combined with a predefined mission profile designed for the MUSV. In each mission segment, resistance was calculated using Series 64 Resistance data, taken from Ship Resistance and Propulsion by Molland [16]. Propulsive power was estimated from this resistance estimate with the following efficiencies applied: hull efficiency - $\eta_H = 1.2$, propeller rotative efficiency - $\eta_{RR} = 0.97$, propeller open water efficiency - $\eta_O = 0.55$, stern tube/bearing/gearbox efficiency - $\eta_{SBG} = 0.98$. Propulsive power estimates were summed with estimated electrical load to determine the total power requirement. This total powering estimate was combined with an estimated specific fuel consumption (SFC = 0.000 196 t/(kWh)) to find the fuel weight for the mission.

The fuel weight and maximum total power outputs from the fuel estimation script, as well as the original design variables, were the inputs for the weight estimation script. This is based on a method detailed in Grubisic 2009 [9], based on a database of similar vessels. Several estimations and assumptions were made to arrive at a weight estimate. Vessel depth was extrapolated from vessel draft. The vessel was assumed to be similar to a patrol craft with

unrestricted service. The structures were assumed to be aluminum. Estimates were made for machinery, outfitting, and electrical equipment weights – these are thought to be the most unreliable due to the highly variable nature of vessels that were included in the database, as well as the novel nature of the MUSV design from a systems perspective. Cargo weight was included in the estimation, however, no weight was allocated for any personnel or provisions. Finally, a rudimentary upright stability estimation was made by approximating the metacentric height of the design. The center of buoyancy (KB) and metacentric radius (BM) were calculated with established empirical fits of similar vessels based on hull parameters. The center of gravity (KG) was much more difficult to estimate, and it was difficult to find regressions or empirical fits. Currently, it is approximated as a factor of draft ($KG = 0.8 \cdot T$).

The design space exploration contains no objectives or constraints, as the driver only generates inputs across the design space specified. The optimization includes both constraints and two objectives. The objectives are to minimize both displacement, and the number of engine starts in the loitering segment. These can be adjusted easily, but the initial choice was aimed at finding a Pareto front between the two objectives.

5.1.1 Inputs

Inputs to the model are provided in two ways. In the design space exploration, a Latin Hypercube generator was used to produce 15,000 samples across the range of input values permitted. The Latin Hypercube generator was chosen because it provided good coverage at the extremes of the design space, which was desired. Other generation algorithms could be used to produce samples. The sampling could potentially also be improved by scaling all variables to the same order of magnitude, although sample coverage was not a notable issue observed.

Table 10: Range of input values used with the model.

Parameter	**Lower Bound**	**Upper Bound**	**Rationale**
Block Coefficient [-]	0.31	0.59	Range of applicability of resistance estimate
Length [m]	25	50	Lower bound from cargo requirements, upper bound from RFP size limit
Beam [m]	3	12	Lower bound from cargo requirements, upper bound large to not limit possible designs
Draft [m]	2	5	Somewhat arbitrary, based on what seemed reasonable
Flywheel Capacity [MJ]	0	1000	Somewhat arbitrary, based on what seemed reasonable

5.1.2 Mission Profile

Details of the mission profile were extrapolated from the MUSV RFP, and based on a 60-day, 4500 nm mission. The profile was generated by assuming the entire range was covered at cruising speed (281.25 h to cover 4500 nm at 16 kn). Each day, it was assumed the vessel would spend one hour in a sprint condition and two hours sensing or communicating. The vessel would be in a loitering condition for the remainder of the mission, not actively stationkeeping or operating but rather using minimal power to observe and report. This mission profile is parametrically defined in `fuelEstimate.py` and can be modified or adapted as seen fit.

Table 11: Details of mission profile used.

Segment	**Speed** [kn]	**Propulsion Power** [kW]	**Auxiliary Power** [kW]	**Time** [h]
Cruise	16	Need to Calculate	300	281.25
Sprint	27	Need to Calculate	300	60
Sense/Communicate	16	Need to Calculate	500	120
Loiter	0	Need to Calculate	5	978.75

5.1.3 Feasibility Constraints

The model, as currently written, has no method for judging the feasibility of the designs it generates. For example, it is entirely possible for the model to generate designs in which the weight significantly exceeds displacement. This means designs must be constrained with various measures. For the optimizer runs, this is quite straightforward as OpenMDAO includes the `.add_constraint()` method. These constraints are applied to the optimizer automatically and can include upper and lower bounds. However, for the design space exploration, the `.add_constraint()` method has no effect because no optimizer is employed. Instead, the entire design space is explored, and infeasible designs are excluded in the plotting script using if-statements. This requires many more samples to be generated than feasible designs that result. For example: 15,000 samples generated by `musvDOEv3.py` led to fewer than 300 feasible designs.

In the current code, the optimization includes more thorough feasibility constraints than the design space exploration. The following constraints are added to the optimization:

- **Weight***: Must be greater than zero
- **Stability**: GM_T must be greater than zero
- **Installed Power**: Must be less than 3000 kW
- **Fuel Weight**: Must be less than 100 t
- **Excess Displacement**: Must have absolute value less than 10 t
- **Engine Runtime***: Must be greater than zero

- **Power Ratio**: Sprint power requirements must be no greater than thrice cruise power requirements

Constraints indicated with a * were added to ensure the optimizer didn't find "zero" solutions that were infeasible. Other constraints were added based on general assumptions of feasibility but can be refined in further iterations of the optimization.

5.2 Incorporating Flywheels into the Model

As demonstrated in Appendix A, FESDs are at a disadvantage to traditional combustion engines in terms of both space and weight. Space and weight are typically analyzed directly and indirectly to determine the "goodness" of a vessel design, so it follows that designs with FESDs would not perform well with the standard analysis. However, FESDs are under consideration not as a replacement for traditional combustion engines but rather for their operational benefits.

FESDs are considered in the fuel estimation component of the model. They are only considered during the loitering period when power requirements are low enough for flywheel discharge to provide sustained power. Two metrics, described in detail below (runtime and number of starts), are calculated for each design given the input FESD capacity. The weight of the FESDs is added to the fuel weight calculated in the fuel estimation.

5.2.1 Flywheel Weight Model

Developing a weight model for FESDs is crucial for their use in the design model, as it allows for the "rubber FESD," which can be sized optimally for each design. An initial weight model was created based on an average of the specific energy for three commercially available or proposed FESDs, listed in Table 12. This works out to a specific energy of roughly 27 $\frac{\text{MJ}}{\text{t}}$, comparable to published estimates of 40 $\frac{\text{MJ}}{\text{t}}$ for commercial FESDs.

Table 12: Characteristics of commercially available flywheels.

	Amber Kin.	**Active Power**	**UT-Austin**
Weight	4536 kg	5103 kg	8600 kg
Speed	10,000 rpm	10,000 rpm	15,000 rpm
Energy	115 MJ	66 MJ	360 MJ

5.2.2 Engine Runtime Metric

The potential for FESDs to support the entire vessel's electrical load in a loitering condition is appealing because it could allow the total shutdown of combustion generators. A runtime fraction, η_{run} is chosen as a measure of time engines must be run in this condition defined in Equation (13).

$$\eta_{run} = \frac{t_{charge}}{(t_{charge} + t_{discharge})} \tag{13}$$

The time engines are running, t_{charge} is defined in Equation (14). N_{fesd} is the number of FESDs on the vessel, and E_{fesd} is the energy capacity of each FESD. P_{cruise} and P_{loiter} are the cruise power requirement (assumed to be close to MCR of the installed engines) and loitering power requirement, respectively. The time engines are not running, and the FESDs are supporting the load, $t_{discharge}$ is defined in Equation (15). Note that both times are defined in terms of one cycle of charge and discharge, with the assumption these would be repeated over the course of the loiter time period.

$$t_{charge} = \frac{(N_{fesd} \cdot E_{fesd})}{(P_{cruise} - P_{loiter})} \tag{14}$$

$$t_{discharge} = \frac{(N_{fesd} \cdot E_{fesd})}{P_{loiter}} \tag{15}$$

Rearranging terms in Equation (16), it is seen that by this definition η_{run} is independent of both capacity and number of FESDs installed. Therefore, η_{run} could be calculated for any design without regard to FESDs and is perhaps less useful in understanding the benefits they provide.

$$\eta_{run} = \frac{\left(\frac{(N_{fesd} \cdot E_{fesd})}{(P_{cruise} - P_{loiter})}\right)}{\left(\frac{(N_{fesd} \cdot E_{fesd})}{(P_{cruise} - P_{loiter})}\right) + \left(\frac{(N_{fesd} \cdot E_{fesd})}{P_{loiter}}\right)} = \frac{\left(\frac{1}{(P_{cruise} - P_{loiter})}\right)}{\left(\frac{1}{(P_{cruise} - P_{loiter})}\right) + \left(\frac{1}{P_{loiter}}\right)} \tag{16}$$

5.2.3 Engine Starts Metric

With a similar goal as understanding engine runtime, an expression for engine starts is developed. A start count, N_{start} is chosen as a measure of time engines must be run in this condition defined in Equation (17).

$$N_{start} = \frac{t_{loiter}}{(t_{charge} + t_{discharge})} = \frac{t_{loiter}}{(N_{fesd} \cdot E_{fesd})\left(\frac{1}{(P_{cruise} - P_{loiter})} + \frac{1}{P_{loiter}}\right)} \tag{17}$$

Notably, the number of times the engines must start can relate inversely to the amount of time the engines must run. This is because less time with the engines running in the loitering condition means the overall cycle time is reduced. A shorter cycle time leads to more charging periods, thus more starts of the engine.

5.3 Results of Initial Explorations

The initial work on the design model was intended largely to set up the model and determine if it was feasible to use OpenMDAO for detailed studies. The results thus far have been positive, with the model producing reasonable designs and the optimization showing results that agree with intuition.

One notable trend observed in results from the design space exploration and optimization was the presence of a Pareto front between vessel displacement, and the number of engine starts in the loitering period. This is seen in Figure 7 and Figure 8. The Pareto front suggests there is a range of optimal values when minimizing both objects, as was expected. The Pareto fronts are relatively steep, indicating that even minimal FESD could significantly reduce the number of engine starts needed.

Generally, results appear somewhat dominated by the feasibility constraints imposed. There is a relatively narrow band of displacements and principal characteristics favored by the model. This, plus the assumed power loads for the mission, would be a good subject to further refine in future studies. Additionally, a better reliability metric would further increase the realism of the trade space. Being able to incorporate the reliability of engine starting and engine run time would allow a Pareto front to be developed between mission reliability and displacement. However, public information on these reliability figures is largely lacking, and engine manufacturers contacted were not willing to share their internal data.

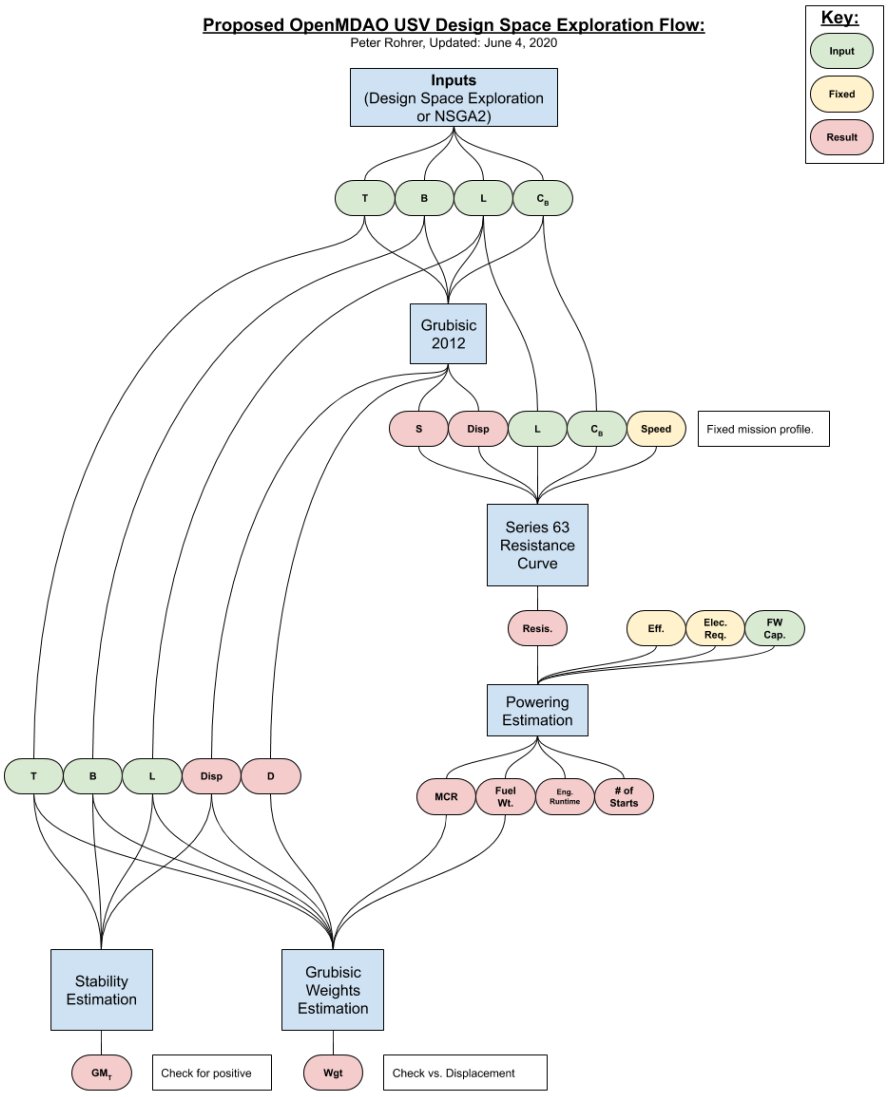

Figure 6: Model Design Flow.

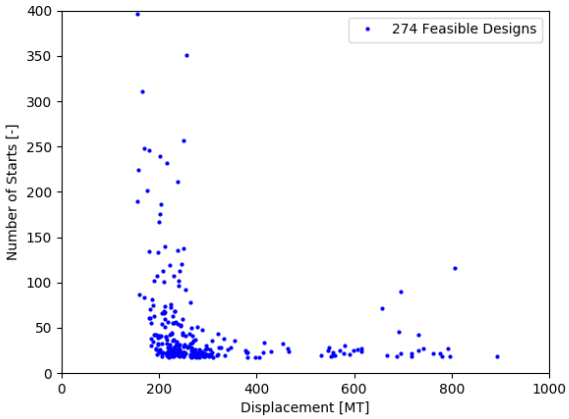

Figure 7: Vessel displacement vs. number of engine starts, design space exploration.

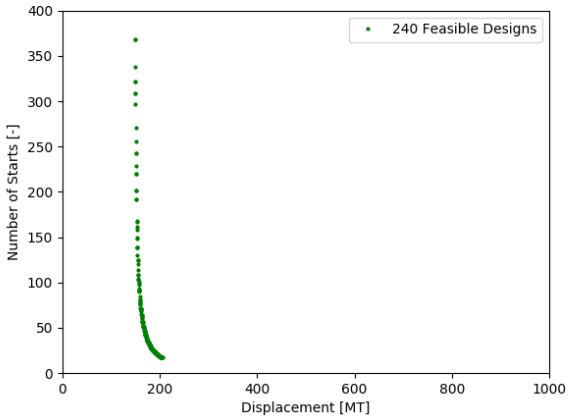

Figure 8: Vessel displacement vs. number of engine starts, optimization.

6 Impact on Ship Motions

While the impact of charge and discharge cycles may be small, both stabilizing or destabilizing gyroscopic moments may be generated by FESD. These forces are explored in this section of the report. Actively controlling the FESD, passively allowing the FESD to rotate, and fixed FESD are considered.

6.1 Flywheel Induced Moments on a Ship

A ship can be outfitted with either a passively or actively controlled flywheel. The main difference between the two is that a passively controlled flywheel is freely allowed to precess about its precession axis and an actively controlled flywheel is forced in precession to generate moments desired to stabilize the vessel[25]. Figure 9 shows the difference between the two setups.

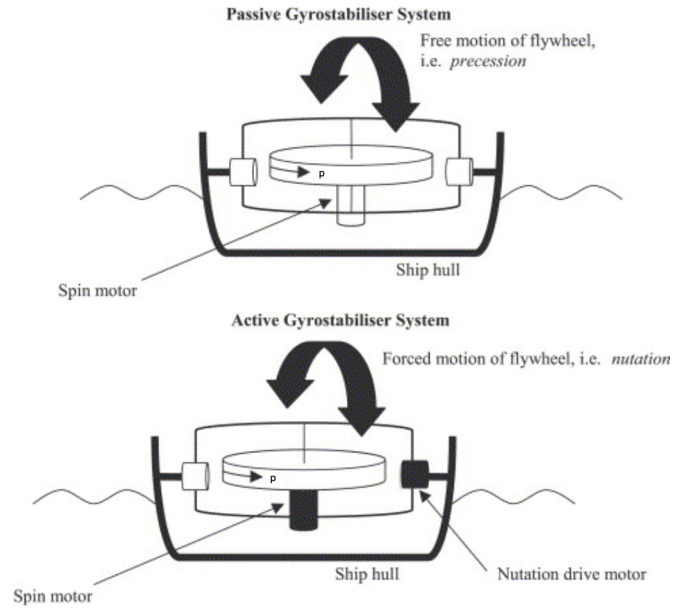

Figure 9: Difference between a passively and an actively controlled flywheel on a ship

These two configurations will both be analyzed throughout this section. For the purposes of this section, it will be assumed that a passively controlled flywheel is outfitted in such a way that it is freely allowed to rotate about its precession axis with negligible friction in the shaft and bearings of the supporting gimbal. It should also be assumed that there is a sensor on the ship that will communicate the changes in vessel motion to the flywheel. Those signals will mainly include the rotation angle and rotation rate of the ship and the flywheel will respond proportionally to those signals.

In general, for a passive flywheel, the precession rate is proportional to the angular rate of motion of the ship. This precession, combined with the conservation of angular momentum of the flywheel, induces a moment that acts in the same direction as the heeling moment of the ship, and both moments work to stabilize the ship. While a passive flywheel precesses

based on the wave environment, an active flywheel is not allowed to precess, or it is only allowed to precess at a programmed rate through a motor, controlled by a computer. This restriction of precession creates a moment that acts in a different direction than the heeling moment.

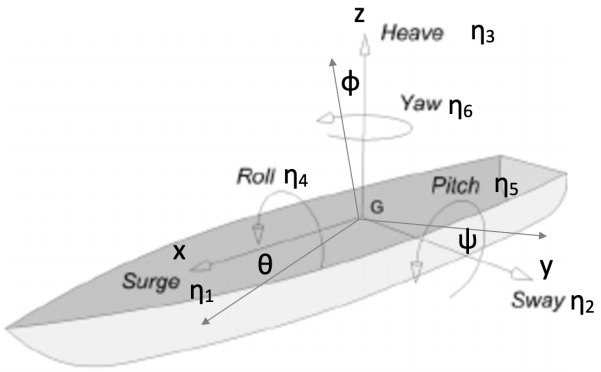

Figure 10: The six degrees of freedom of ship motion

Positive rotational motion will be defined using the right-hand rule of the axis that the ship is rotating about. Roll motion will be positive to starboard and defined as an angle ϕ. Pitch motion will be positive bow down and defined as angle θ. Yaw motion will be positive counter-clockwise when viewed from above ψ. The degrees of freedom are represented as η_j, where j=1-6 are surge, sway, heave, roll, pitch, and yaw, respectively.

Using basic marine dynamics concepts, the vessel's motions can be quantified using Equation (18).

$$\{-\omega_e^2(M_{jk} + A_{jk}) + i\omega_e B_{jk} + C_{jk}\}\zeta_k = F_j \tag{18}$$

In this general equation, ω_e is the wave encounter frequency, M_{jk} is the mass matrix, A_{jk} is the added mass matrix, B_{jk} is the damping matrix, C_{jk} is the restoring force matrix, ζ_k is the motion vector, and F_j is the forcing vector. Depending on the degrees of freedom involved, both j and k can vary from 1 to 6. For example, B_{45} is the damping force coefficient in roll, due to unit displacement in pitch. The vector ζ_k can range anywhere from 1 to 6, with $\zeta_4 = \phi$, $\zeta_5 = \theta$, $\zeta_6 = \psi$.

The dynamics of flywheels will have to be incorporated into these equations of motion and the purpose of this section is to determine the level of impact those additional dynamics have on the seakeeping of a ship.

6.1.1 Passively Controlled Flywheels

A passively controlled flywheel is able to freely precess about its precession axis, and its precession rate is dependent upon the motion of the ship. The case of a flywheel with spin

axis in the vertical direction on a ship encountering roll motion will be used to describe the general induced passive flywheel moment. To clarify, the following passive flywheel is able to rotate about its spin axis (z-axis), its precession axis (y-axis), but not about the x-axis. As the ship rolls, the flywheel and its supporting structure will also roll.

Conceptualization

For a vessel encountering waves that cause it to roll, a passive flywheel with a vertical spin axis will create a moment in the opposite direction of the environmental roll moment, which will stabilize the vessel[18]. Figure 11 shows a cross-subsection of a vessel looking from the stern. The vessel is rolling starboard, or clockwise, which means it has a positive roll. A flywheel on the deck of the ship is spinning clockwise when viewed from above with rotational velocity ω (the results will be the same no matter the spin direction of the flywheel). This means that its angular momentum H points in the negative z-axis. A wave traveling from port to starboard creates a force on the hull which induces an environmental roll moment on the vessel that causes it to roll positive to starboard. The environmental roll moment τ_{roll} will follow the right-hand rule of this roll motion, which means that τ_{roll} points into the page.

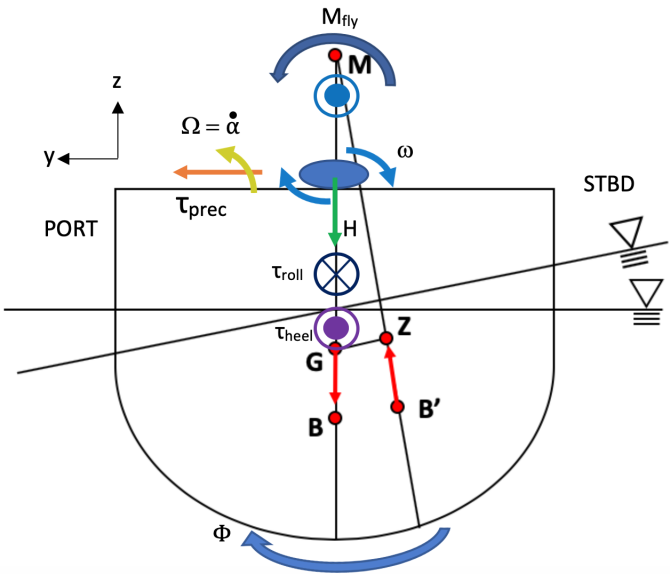

Figure 11: Astern view of a ship rolling positive starboard ϕ and resulting forces and moments with a passively controlled flywheel

Due to this roll motion, the angular momentum vector H of the flywheel has to change and will point slightly to the left, or port, instead of straight down. Conservation of angular momentum wants to keep H pointing downwards, and because the flywheel is forced to roll, the flywheel will rotate about another axis. In this case, it will rotate about its precession axis, which is the ship's pitch axis. Using Equation (10), the direction of precession can be determined. However, the roll moment of the ship should not be used as the τ in this equation.

The torque that is providing the offset of forces, as shown in the wheel example and the

mathematical rotor, is the heeling moment of the ship. When the ship rolls to starboard, the center of buoyancy B shifts starboard to B', because there is more submerged volume on the starboard side of the vessel than the port side, as shown by the new slanted waterline in Figure 11. The center of gravity, or the weight of the vessel, never changes because it is assumed that the vessel rotated about the center of gravity, which only caused the center of buoyancy to shift. Using the right hand rule, the torque created by the offset of the new buoyancy force B' and the weight G, is τ_{heel}[13], which points out of the page, and should be used to determine the direction of precession. In general, $\tau_{heel} = -\tau_{roll}$.

The direction of precession is, therefore the cross product between H and τ_{heel}, which points port. The right-hand rule also says that since the precession vector is positive port, the flywheel will precess with positive pitch (rotate into the page, bow down). The precession velocity is proportional to the roll rate of the vessel due to the roll moment from the waves [23], which is unknown for the time being, but will be explained in the next subsection.

Finally, using Equation (12), the moment that the flywheel induces on the ship is the cross product between the precession velocity (port) and the spin velocity (down), which results in a counter-clockwise moment M_{fly} that points out of the page and stabilizes the vessel[2].

Calculation
Rewriting Equation (18), the roll motion of a ship encountering beam waves can be expressed as Equation (19) where I_{44} is the moment of inertia of the ship in roll due to roll motion, B_{44} is the roll damping force coefficient due to roll motion, C_{44} is the roll restoring force coefficient due to roll motion, τ_{roll} is the wave-induced roll moment, n is the number of flywheels on board, H is the angular momentum of the flywheel, ϕ is the roll motion of the vessel, and α is the precession motion of the flywheel [18]. The I_{44} term is assumed to include the added mass of the ship in roll, the number of flywheels, in this case, is one so $n = 1$, and the second term on the right side of the equation is M_{fly}.

$$I_{44}\ddot{\phi} + B_{44}\dot{\phi} + C_{44}\phi = \tau_{roll} - nH\dot{\alpha}cos(\alpha) \tag{19}$$

As explained before, the moments important to these calculations in roll are the wave-induced roll moment τ_{roll} and the moment of the flywheel M_{fly} (τ_{heel} is included within the hydrostatic force in C_{44}). The $M_{fly} = nH\dot{\alpha}cos(\alpha)$ term on the right side of the equation is similar to Equation (12) where the angular momentum $H = Ip$ is multiplied by $\Omega = \dot{\alpha}$ ($M_{fly} = Ip\Omega$)[2].

The cosine of the precession angle is due to the fact that the flywheel precesses about the pitch axis. Only the cosine of the precession velocity can be used to be crossed with the spin angular velocity to create a moment that is two-dimensionally counter-clockwise[2]. Therefore, as the flywheel precesses it develops another component of angular momentum, which will induce a separate moment that will be discussed in a later section. For small angle approximations, $\cos\alpha = 1$ and $\sin\alpha = \alpha$ and so $M_{fly} \approx nH\dot{\alpha}$.

Sensors relay the roll rate of the ship to the flywheel and the precession velocity is proportional

to the roll rate of the vessel [18][22][23]. Equation (20) describes the motion of the flywheel during precession where I_g is the moment of inertia of the flywheel about its precession axis, B_g is the damping force coefficient of the flywheel, C_g is the restoring force coefficient of the precessing flywheel, τ_p is the precession control torque, α is the precession angle, and ϕ is the roll angle [18].

$$I_g\ddot{\alpha} + B_g\dot{\alpha} + C_g sin(\alpha) = H\dot{\phi}cos(\alpha) + \tau_p \tag{20}$$

The first term on the right side of the equation is considered the precession torque $\tau_{prec} = H\dot{\phi} = Ip\dot{\phi}$, while the second term on the right side is the precession control torque τ_p. For a passive flywheel, τ_{prec} describes the torque induced in the precession frame, but since the flywheel can freely precess, it is not included in the overall ship equations of motion. A passive flywheel also has no controller, so $\tau_p = 0$[2].

As seen in Equation (12) and Equation (19), M_{fly} is a function of precession velocity $\dot{\alpha}$. However, Equation (20) says that precession velocity is a function of roll rate $\dot{\phi}$. Therefore, M_{fly} cannot be calculated until the roll rate of the ship is known [23].

The precession rate can be considered proportional to the roll rate of the vessel $\dot{\alpha} = q\dot{\phi}$ where q is a constant. This proportionality can be substituted into Equation (19) for $\dot{\alpha}$ in the M_{fly} term and rearranged to look like Equation (21)[18].

$$I_{44}\ddot{\phi} + [B_{44} + nHq]\dot{\phi} + C_{44}\phi = \tau_{roll} \tag{21}$$

The M_{fly} term was combined into the B matrix because after the substitution, it is also proportional to the roll rate $\dot{\phi}$ of the ship.

6.1.2 Actively Controlled Flywheels

An actively controlled flywheel is not able to freely precess about its precession axis. Rather, its precession is programmed by a separate drive motor. This forced precession motion is called nutation, as seen in Figure 9. This restriction of free precession creates other moments on a ship. The same case of a vertical spin axis flywheel on a rolling ship will be used to first explain the general induced moments.

For the following example, it should be noted that an actively controlled flywheel is not allowed to freely precess, meaning that it is outfitted with the proper gimbal and support structure that eliminates rotation about the athwartship axis (port to starboard axis). It is also assumed that it has a nutation drive motor that can be controlled by a computer however no precession control is applied ($\tau_p = 0$), so the flywheel will not nutate.

Conceptualization

For a vertical spin axis active flywheel on a rolling ship, the induced flywheel moment works about the pitch axis instead of the same roll axis as before. Figure 12 is adapted from Figure 11 to account for an active flywheel. It is the same ship cross-section and has the same flywheel spinning with rotational velocity ω, which creates an angular momentum H in the negative z-axis. The same wave induces positive roll motion and creates a torque τ_{roll} that points into the page.

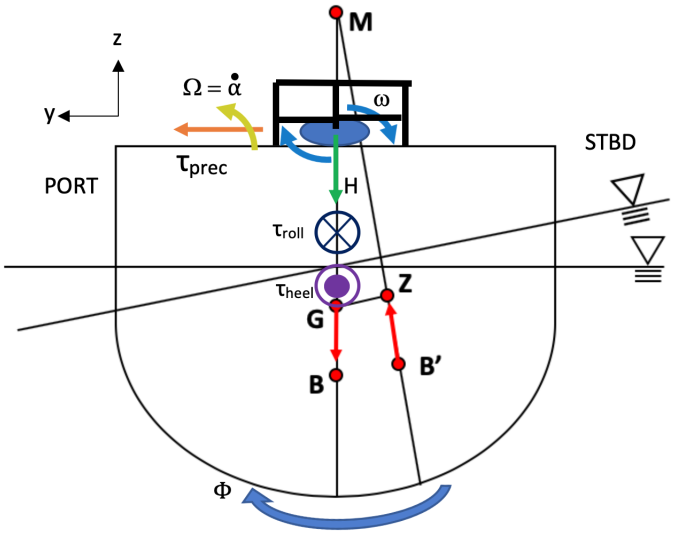

Figure 12: Astern view of a ship rolling positive starboard ϕ and resulting forces and moments with an actively controlled flywheel

Conservation of angular momentum will want to stay pointing in the negative z-axis, so this roll motion will want to make the flywheel precess about the pitch axis, as explained in the passive flywheel section. The direction of this precession will also be the same, due to the same explanation of using the cross product of H and τ_{heel}. However, an active flywheel is not allowed to precess about its precession axis. The conservation laws are satisfied by creating an induced torque through the support structure of the restricted flywheel and through the whole ship that acts about the pitch axis[2].

The induced moment is seen in Figure 12 as τ_{prec} that points in the port direction (positive y-axis) and acts in the positive pitch direction (into the page, bow down). Since there is no precession, Equation (12) cannot be used to quantify this moment. However, it is assumed that there is a "hidden" precession velocity that the flywheel wants to attain, which is proportional to the ship roll motion and will be used to quantify the active flywheel induced moment τ_{prec}. The precession torque is not included in the passive flywheel case because it is assumed that the torque does not have an effect on the ship as a whole and only is a factor in the precession equations of motion.

Calculation

Equation (19) can also be used for an actively controlled flywheel, but it is rewritten into

Equation (22) with all the same variables as a passive flywheel[18].

$$I_{44}\ddot{\phi} + B_{44}\dot{\phi} + C_{44}\phi = \tau_{roll} + \tau_{prec} \tag{22}$$

Equation (20) is rewritten for no precession motion, which yields Equation (23).

$$0 = H\dot{\phi} + \tau_p \tag{23}$$

The first term on the right side is the precession torque $\tau_{prec} = Ip\dot{\phi}$, which is the product of the angular momentum of the flywheel H and the roll rate of the ship $\dot{\phi}$. This is equal to the actively controlled flywheel-induced moment on a ship that acts about the pitch axis. If the flywheel nutation motor is not being controlled, then $\tau_p = 0$, but if not, then the control signal would be equal and opposite to the precession torque, to cancel out the induced pitch moment.

Similarly to the passive flywheel, the active flywheel induced moment τ_{prec} cannot be calculated until the roll velocity of the ship is known[23]. The roll velocity will be calculated using a program called SHIPMO which will be explained in a later section.

When the flywheel is fixed in place on the ship, the induced precession torque is an extra external moment that can be added onto the right side of Equation (22), and rearranged to form Equation (24).

$$I_{44}\ddot{\phi} + [B_{44} - nHq]\dot{\phi} + C_{44}\phi = \tau_{roll} \tag{24}$$

Similarly to a passive flywheel, the flywheel-induced moment is proportional to the roll velocity and is combined into the B matrix[23]. The next step is to determine the elements of the B matrix that are affected by these extra flywheel moments.

6.1.3 Matrix Modifications

Matrix Definition
Since all the previously mentioned flywheel moments are proportional to the rotational velocity of the ship, all the flywheel moments have to be added to the B matrix of the ship's equations of motion. The 6-by-6 damping coefficient matrix is shown below in Equation (25) and represents the damping force coefficients for a ship in the ith direction, due to unit rotation in the j direction. For example, B_{54} is the damping force coefficient in pitch (5), due to unit rotation in roll (4).

$$B_{ij} = \begin{bmatrix} B_{11} & B_{12} & B_{13} & B_{14} & B_{15} & B_{16} \\ B_{21} & B_{22} & B_{23} & B_{24} & B_{25} & B_{26} \\ B_{31} & B_{32} & B_{33} & B_{34} & B_{35} & B_{36} \\ B_{41} & B_{42} & B_{43} & B_{44} & B_{45} & B_{46} \\ B_{51} & B_{52} & B_{53} & B_{54} & B_{55} & B_{56} \\ B_{61} & B_{62} & B_{63} & B_{64} & B_{65} & B_{66} \end{bmatrix} \tag{25}$$

These damping force coefficients, when multiplied by a rotational velocity, resulting in a damping force on the vessel.

The following sections discuss which elements of the B matrix are affected by flywheel-induced moments in three different flywheel orientations, in three different rotational degrees of freedom. Since this analysis will only involve j displacements (4, 5, and 6) and those j displacements will only have an effect on the ith directions 4, 5, and 6, then only the bottom right quadrant of the B matrix will have flywheel induced terms (Equation (26)).

$$B_{ij} = \begin{bmatrix} B_{44} & B_{45} & B_{46} \\ B_{54} & B_{55} & B_{56} \\ B_{64} & B_{65} & B_{66} \end{bmatrix} \tag{26}$$

For the purposes of this paper, the flywheel-induced moment terms that will be added to the B matrix will be represented as F_{ij} where $M_{fly_{ij}} = F_{ij}\dot{\zeta}_j$ where $\dot{\zeta}_4 = \dot{\phi}$, $\dot{\zeta}_5 = \dot{\theta}$, or $\dot{\zeta}_6 = \dot{\psi}$. The next few sections will discuss the modifications to the B matrix for three different orientations of the flywheel.

In summary, $F_{ij} = nHq$ for a passive flywheel case and $F_{ij} = -nHq$ for an active flywheel case.

6.2 Code Implementation (SHIPMO)

This section will be used to show the seakeeping effects that flywheel-induced moments have on ships using a seakeeping prediction program called SHIPMO, which was developed by Professor Robert F. Beck and Professor Armin W. Troesch at the University of Michigan. This section will also serve as a guide to the procedure that was done to complete this analysis so that future work can be completed easily. SHIPMO is written in Fortran77 and computes ship motion in all degrees of freedom using strip theory, which is a method of modeling a ship as a sum of many strips, or cross-sections. This program will be run for a given ship, the *USS Ann Arbor*, without any flywheels, and then run with flywheels in all orientations described in the previous section. The program will output response amplitude operators (RAOs) for the ship with no flywheels and then for the ship with flywheels. The magnification of these RAOs will be able to determine the seakeeping effects that flywheels have on the ship.

6.2.1 Magnification Curves (RAOs)

The general equations of motion for a ship undergoing six degrees of freedom can be described by Equation (27) where m is the 6x6 mass matrix, A_{ij} is the 6x6 added mass matrix, B_{ij} is the 6x6 damping matrix, C_{ij} is the hydrostatic restoring matrix, F_{ex} is the sum of the external forces on the ship, ζ_j is the motion in the degree of freedom j, which corresponds to the degrees of freedom in Figure 10, and the dots represent the time derivative of the motion.

$$[m + A_{ij}]\ddot{\zeta_j} + B_{ij}\dot{\zeta_j} + C_{ij}\zeta_j = F_{ex} \tag{27}$$

By outfitting the ship with flywheels, a B_{fly} matrix can be added to the B matrix, which the theory is explained in the previous section. Assuming harmonic motions with $\zeta_j = Ae^{i\omega t}$, Equation (27) can be rewritten as Equation (28), which is shown again below where F_j is a complex matrix.

$$\{-\omega_e^2(M_{jk} + A_{jk}) + i\omega_e(B_{jk} + B_{fly-jk}) + C_{jk}\}\zeta_k = F_j \tag{28}$$

Solving Equation (28) for ζ_j and dividing both sides by the external force amplitude (wave amplitude) yields the response amplitude operator of the ship in the six degrees of freedom. The plot of this value versus a range of wave frequencies is the RAO curve, which is one of the outputs of SHIPMO. If the RAO curve spikes at a certain value, that means that there is a large motion in that degree of freedom due to that excitation frequency. The goal of this analysis will be to determine how the spike, or the overall magnification of the curve, changes with the addition of flywheels on the ship. Before the program is run, it is helpful to first document how the program can be run on a computer.

6.2.2 Setup on Mac

SHIPMO can be run on Windows (most commonly done on the CAEN computers in the Naval Architecture and Marine Engineering building on U of M's campus) by using three files: the executable (shipmo.exe), which was compiled from the SHIPMO source code (shipmo.bm.v1.2.f), the input file (SHIPMO.IN), and a G2S1.3 file. When these three files are in the same folder and the executable is run, an ADMASS file, a POT file, an RAO file, a SHIPMO.OUT file and a visc file will be output. The contents of each file can be found by reading the SHIPMO User Manual [1] and Appendix B, but the main concern will be the RAO output file, which contains the magnification curve for various frequencies.

If, however, the user has to run the program on MacOS, the following procedures must be taken. Three items are needed before SHIPMO can be run on Mac:

1. The SHIPMO source code: "shipmo.bm.v1.2.f"

This is the main code that Professors Beck and Troesch wrote to compute the seakeeping motions of a vessel (permission from the professors is needed). It is about 7680 lines long and references many subroutines and functions to make the seakeeping calculations. Details on these subroutines can be found in Appendix C.

2. A text editor

   A recommended text editor for future analyses like this one is "Atom", which is free online, and after installing the ide-fortran library and language-fortran libraries, the SHIPMO code is much easier to read and understand.

3. A fortran compiler

   To download and execute the correct fortran compiler on Mac, the following steps can be taken.

   (a) Download the gfortran code at:
   http://hpc.sourceforge.net/

   (b) That link will direct the user to a HPC page with multiple gcc and gfortran binaries for various MacOS versions. Click on the "gcc" link for the operating system the user is using (at the time this was written, Catalina was used). The user will be directed to another page where it will automatically start downloading the gcc package. Even though it says "gcc", the gfortran compiler is also included.

   (c) Once it has downloaded, open the terminal and type "cd Downloads", or "cd wherever the gcc package downloaded to". Then type in the terminal "gunzip gcc-9.2-bin.tar.gz" if the browser did not already unzip the file.

   (d) Then type in the terminal "sudo tar -xvf gcc-9.2-bin.tar -C /", which will put the "usr" folder that was downloaded into the location of the computer where it will work. This can be checked by navigating through, or changing, the directories by typing "cd /", which navigates to the root directory, then "cd usr", then "cd local", then "cd bin". Typing "ls" for list will then show all that is in that folder and "gfortran" should be listed. Other useful tips: "cd tilde" navigates to the home directory, "cd .." navigates up one directory level, and "cd -" navigates to the previous directory.

Once the fortran compiler is setup, the SHIPMO code can be compiled and executed. Once the user has formatted the SHIPMO.IN file and the source code file to their liking, the following steps can be taken to produce results.

1. Create a folder or location that includes three files: a SHIPMO.IN file, a G2S1.3 file, and the source code file (shipmo.bm.v1.2.f).

2. Open the terminal and navigate to that location by typing "cd [filepath to SHIPMO files]"

3. Type "gfortran -fno-bounds-check -o shipmo _"your initials".exe shipmo.bm.v1.2.f" to create the executable shipmo _"your initials.exe" based on the input file "shipmo.bm.v1.2.f". The new .exe file should show up in the folder.

4. Type “chmod +x shipmo _“your initials”.exe”

5. Type “./shipmo _”your initials”.exe” to run the executable file and the output files will show up in the folder.

Once the output files are created, seakeeping analysis can be done. The following sections will discuss how the input file and source code was modified for the addition of flywheels for a certain ship.

6.2.3 Ship Selection

The ship that was chosen for this analysis is based on the analysis done by Joseph Van Houten’s master’s thesis [25]. Detailed characteristics of U.S. frigate vessels are not publicly available, so a variation of a U.S. frigate vessel was created, the *USS Ann Arbor*, and its hull characteristics are listed in Table 5.

6.2.4 Code Modifications

Most of the code in this analysis was adapted from Joseph Van Houten’s master’s thesis. This was done because Joey had developed a new source code version that was compatible to read in various flywheel data, so not much more needed to be changed. For example, Van Houten added a couple of lines of code to read in the flywheel data, which will be discussed later in this section. With this flywheel source code already set up, all that needed to be changed was the addition of the B_{fly} matrix, according to the various flywheel scenarios discussed in the earlier section. The input file (SHIPMO.IN) was also adapted from Van Houten’s work and has the ability for the user to easily change various flywheel variables, such as the number of flywheels, the rotor moment of inertia, or even the orientation of flywheels on board.

6.2.5 SHIPMO.IN

Modifications were made to the source code and the input file in this analysis. The input file, SHIPMO.IN, declares the setup for the model undergoing simulation, such as what preferences the user desires, initializing variables, and modeling the geometry of the ship. Appendix B describes what each line of the input file does to set the preferences of the model. Two main parts of the SHIPMO.IN file were modified to account for the addition of flywheels.

1. The control variable line (the second line) usually has 15 inputs. A 16th input (IP) is added to the end of this line to tell the source code whether or not the ship has flywheels. If IP = 0, then there are no flywheels on board. If IP $\neq$ 0, then there are flywheels on board.

2. Another line is added below the third line. This is what is called the flywheel variable line. This line takes as input, in order, the number of flywheels on board n (IFLYS), the flywheel rotational velocity ω (AVR), the flywheel moment of inertia about its spin axis I (ROTINT), the flywheel moment of inertia about its precession axis (PREINT),

the flywheel transverse center of buoyancy (FLYTCB), and the flywheel longitudinal center of buoyancy (FLYLCB)

Only IFLYS, AVR, and ROTINT were used in this analysis. Van Houten had used PREINT, FLYTCB, FLYLCB in his previous analysis and they were still included in the code.

Again, Appendix B lists what each line in the SHIPMO.IN file means and what preferences this simulation has. In summary, for this simulation, the second line says that the ship encounters regular waves (ID=0), both vertical and horizontal planes are considered (IE=1) so all degrees of freedom are considered, the ship encounters long-crested waves (IF=0), and the ship is divided into 20 stations (NS=20). The third line lists the ship length, the standard density of salt water, gravity, the standard viscosity of salt water, the displacement of the ship, and the depth of the water (the value 0 means infinite depth). The fourth line lists the variable flywheel characteristics, which can be shown in Table 13 [7].

Table 13: Flywheel characteristics

Parameter	**Value**
Mass	2,300 kg
Diameter	1.32 m
Moment of Inertia	389 kg-m^2
Rotational Velocity	7,000-15,000 RPM
	733.04 - 1570.79 rad/s
Overall Volume	20 m^3
Overall Deck Area	2.5 m^2

The number of flywheels is variable but will only change by orders of magnitude in this analysis, the rotational velocity and moment of inertia are found in Table 13, PREINT is set to 400 kg-m^2, FLYTCB is set to 0.1 m, and FLYLCB is set to 1 m. The bulk of the input file models the geometry of the ship at each station and was taken from Van Houten's analysis. The second to last line lists the wave amplitude (1 m), the wavelength or wave frequency start, end, and their increment, and then the ship speed start, end, and increment (ship speed is constant). The last line lists the wave angle heading start, end, and increment (headings from 0 to 180 degrees by 45 degree increments).

A couple notes: First, when horizontal and vertical planes are mentioned, the horizontal plane is degrees of freedom surge (1), heave (3), and pitch (5), and the vertical plane is degrees of freedom sway (2), roll (4), and yaw (6). Secondly, two SHIPMO.IN files are needed for one analysis. One file creates frequencies between 0.25 and 0.78 rad/s. The other file creates frequencies between 0.79 and 2.77. There is room for future work to create a single SHIPMO.IN file to read in the desired frequencies by altering the second to last line. That was not done for this analysis because Van Houten created a MATLAB file "Rao_Graph.m" that reads in an Excel sheet with one sheet for the first SHIPMO.IN file and the second sheet for the second SHIPMO.IN file.

More details about the SHIPMO.IN file can be found in the SHIPMO User Manual [1]. Once

the two SHIPMO.IN files are created to the user's liking, it can be placed in the same folder as a G2S1.3 file, as well as the source code, and be compiled to produce output files.

6.2.6 Source Code

The source code is the main code that performs all the functions that calculate the ship motions with the given inputs. The original code is named "shipmo.bm.v1.2.f" and is about 7,860 lines long. Access to the original source code was given by one of its creators, Professor Armin Troesch. This section will explain the modifications made to the source code to account for flywheels, as well as a record of what procedures were done in this analysis to be referenced for future analysis.

The purpose of this analysis was to determine what effects flywheels have on the seakeeping performance of a ship, based on an additional B_{fly} matrix. All that needed to be done was append a couple F_{ij} terms to the B matrix of the original source code, except that the original source code was not capable of reading in flywheel data. In his source code versions, Van Houten had modified the source code to be compatible with flywheel data. However, the later versions of the source code had many changes to account for flywheels, such as adding an entire subroutine called FLYWHL to calculate flywheel dynamics. A good topic for future work would be to expand upon the FLYWHL subroutine in fortran to account for flywheels, but that is not in the scope of this section.

To modify an existing flywheel-compatible source code that does not have too many changes from the original source code, the "shipmo3.bm.v1.2.f" was chosen to be further modified for this analysis. The changes made to the shipmo3 source code are as follows:

1. The additional C matrix around line 887 was commented out since this analysis does not have any changes to the C matrix.
2. There is a section around line 4,900 that deals with the coupling or uncoupling of the vertical and horizontal planes. It's easier for calculations if the planes are uncoupled (DOF 2,4,6 do not depend on DOF 1,3,5) but this analysis requires that the planes be coupled because, in most flywheel scenarios, there is at least one term that depends on both planes (i.e. a F_{45} or F_{56} term). The section of the source code that calculated the decoupled motion was commented out and the coupled motion section remained.
3. The B_{fly} matrices were added to the B matrix around line 4,300 in the subroutine that calculated the added mass and damping coefficients. For example, if the flywheel scenario had a F_{44} term, then the expression (IFLYS*AVR*ROTINT) was appended to the B_{44} term in the subroutine.

Therefore, since there are 9 different flywheel scenarios (3 fixed axis flywheels for 3 different spin axis orientations), 9 source codes can be created, one for each of the flywheel scenarios. The SHIPMO.IN case would not change between the flywheel scenarios, as long as IP $\neq 0$ at the end of the second line. Another method that could have been done was only having

one source code with an if statement for the B matrix. The IP placed in the input file could range between 1 and 9 for each flywheel scenario and that would determine which part of the if statement was called to produce its necessary B matrix. This would again be a good topic for future work that wasn't necessary for this analysis.

6.3 Induced Moments Due to External Forces

A flywheel with a vertical spin axis can be fixed on a ship in three different directions or axes. Each of those three fixed axes will each undergo motion in the three rotational degrees of freedom. This section will cover the case where the flywheel's fixed axis is in the y-axis, or the athwartships axis. For this analysis: FIXED AXIS = Y-AXIS, SPIN AXIS = Z-AXIS.

Roll A vertical spin axis and athwartships (port to starboard) precession axis flywheel undergoing roll motion is the same as the passive flywheel example in the previous section. We know from this example that the flywheel-induced moment acts in the same direction as the ship-heeling moment to stabilize the ship in roll. However, there is an additional induced moment in another direction due to this motion. Figure 13 shows how a yaw moment is created for this flywheel orientation.

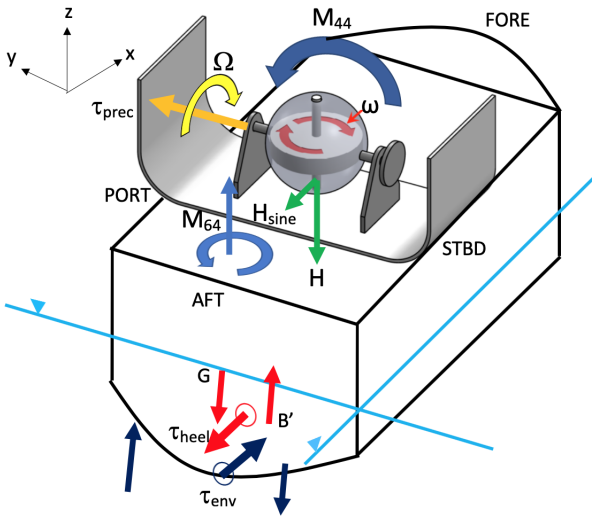

Figure 13: Z-Spin and Y-Fixed flywheel-ship schematic of the induced flywheel moments due to roll motion

To reinforce the learning of the previous section, a passive flywheel with a vertical spin axis is outfitted on a ship so that it can rotate along its spin axis (z-axis), its athwartship axis (y-axis), but not its centerline axis (x-axis). It is spinning with a clockwise rotational velocity ω, which gives it an angular momentum H in the downward direction.

Again, there is a wave that hits the vessel from port to starboard that causes the vessel to roll positive starboard. This wave force essentially creates a moment, which was previously named τ_{roll}, but will from now on be considered the environmental moment or torque τ_{env}

($\tau_{roll} = \tau_{env}$), which points in the positive x-direction. This environmental torque shifts the underwater volume to the point B', which means that the heeling moment of the ship τ_{heel} points in the negative x-direction. This was the torque used to determine the direction of the precession of the flywheel. Equation (10) should technically be written as Equation (29) since τ_{env} is the correct moment to use to determine the direction of precession. It just so happens that direction-wise, $\tau_{env} = -\tau_{heel}$ in this case, which is why the direction of τ_{heel} was used in Equation (10).

$$PrecessionDirection(\Omega) = H \times -\tau_{env} \tag{29}$$

1. Using Equation (29), the direction of precession points in the positive y-direction, which means that as the ship rolls, the conservation of angular momentum will cause the flywheel to precess positive around the y-axis (bow down). Then, using Equation (12), the flywheel-induced moment stabilizes the vessel in roll due to roll, giving it a subscript of M_{44}. This moment is technically negative since it acts opposite to positive roll ($M_{44} = -F_{44}\dot{\phi}$).

2. An important aspect that was left out of the previous analysis is that as the flywheel precesses, the angular momentum also precesses with the flywheel and develops a component in the negative x-direction. This will be referred to as the H_{sine} term. This component of angular momentum will create a different moment on the vessel. Using Equation (12) again, the resulting moment points up and rotates counterclockwise. This is a positive M_{64} term since there is a moment about the positive yaw axis, due to rotation in roll.

3. Another important factor is the direction of the spin of the flywheel. When it spins clockwise, H points in the negative z-direction. When the flywheel spins counterclockwise, H points in the positive z-direction. This does not change the direction of M_{44}, but it does change the direction of M_{64}.

   If the flywheel were to spin counterclockwise, Equation (29) states that the precession direction then points starboard, and the flywheel will precess the other way (bow up). Using Equation (12), the main flywheel-induced moment M_{44} will still point in the negative z-direction and act in the same direction as the heeling moment to stabilize the ship. The small H_{sine} term of the precessing angular momentum will again, point in the negative x-direction, but the resulting moment calculated by Equation (12) will point downwards, opposite of the M_{64} term in the previous analysis.

   To counteract the induced yaw moment of the vessel, two flywheels can be outfitted on the ship, each with opposite directions of spin. Their resulting yaw moments will be equal and opposite to each other and cancel out unwanted yaw moments.

In summary, this flywheel orientation undergoing roll motion will create a moment in roll due to roll (M_{44}), and a moment in yaw due to roll (M_{64}), but no moment in pitch due to

roll (M_{54}=0). If an even number of flywheels n are outfitted with $n/2$ flywheels spinning clockwise and $n/2$ flywheels spinning counterclockwise, the M_{64} terms will cancel each other out. For the purposes of this section, we will consider that all n flywheels on board will be spinning in the same direction.

Mathematically, $M_{44} = -F_{44}\dot{\phi} = -nHq\dot{\phi}cos(\alpha)$, $M_{64} = F_{64}\dot{\phi} = -nHq\dot{\phi}sin(\alpha)$, and $M_{54} = 0$, for a flywheel with its angular momentum pointing in the negative z-direction. These become the M_{fly} terms that appear on the right side of the equations of motion, as shown by Equation (19), and need to be moved to the left side of the equation as shown by Equation (21), since the M_{fly} term depends on the roll rate of the ship. Therefore, the F_{44} term is positive and the F_{64} term is negative, in the case where the flywheel's angular momentum H is pointing downwards.

Pitch The same flywheel setup undergoing pitch motion is the same as the active flywheel example in the previous section. Using the same variables and directions as the roll section, Figure 14 shows the responses of the setup in pitch.

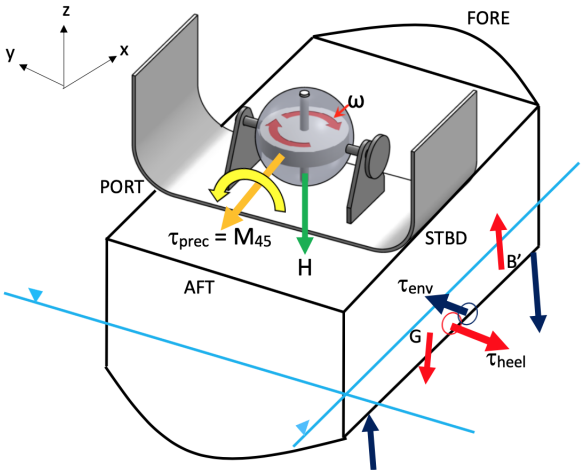

Figure 14: Z-Spin and Y-Fixed flywheel-ship schematic of the induced flywheel moments due to pitch motion

The environmental moment τ_{env} rotates the ship in positive pitch (bow down) and points in the positive y-direction, while the heeling moment τ_{heel}, that comes from the increase in underwater volume towards the bow, acts in the negative y-direction. To conserve angular momentum, Equation (29) states that the flywheel will precess about the negative x-direction. However, the way this vertical axis flywheel is set up, it can only precess about the y-axis and not the x-axis. This is the case of an active flywheel, except that it cannot even be nutated in this direction. Nutation is computed control over precession, which is still about the y-axis in this case. This flywheel wants to precess about the negative x-direction, which it is not set up to do. This restriction of precession results in a moment in the roll direction due to pitch motion. More mathematically, this would be an induced M_{45} term and would be negative since it points in the negative x-direction. This is the same as the precession

torque τ_{prec} mentioned in the active flywheel section.

It should be noted that in this case of H pointing in the negative z-axis, τ_{prec} is also negative, so the signs of both terms should be the same. However, when the τ_{prec} term is plugged back into Equation Equation (22), it must change sign to switch to the left side of the equation, as shown by Equation Equation (24). In short, τ_{prec} is the same sign as H in this flywheel setup, but F_{45} is the opposite sign of H.

When the flywheel is spinning in the counterclockwise direction (positive) in this case, the flywheel will want to precess about the positive x-axis to conserve angular momentum (Equation Equation (29)). This means that τ_{prec} also points in the positive x-direction, but F_{45} would be the opposite sign, or negative, when used in the final B_{fly} matrix.

There is no yaw-induced moment due to pitch for this flywheel with its precession axis in the y-direction because the flywheel is not allowed to precess and so there is no H_{sine} term to create a yaw-induced moment.

Yaw The third degree of freedom that is rotated in this setup is yaw. As seen in Figure Figure 15, there is an environmental torque that is applied on a ship. This torque is shown by the two dark blue arrows that cause the ship to yaw in a positive direction. τ_{env} then points in the positive z-direction and the resulting cross product of the angular momentum H (down) and $-\tau_{env}$ (down), is zero since those two vectors are in the same direction.

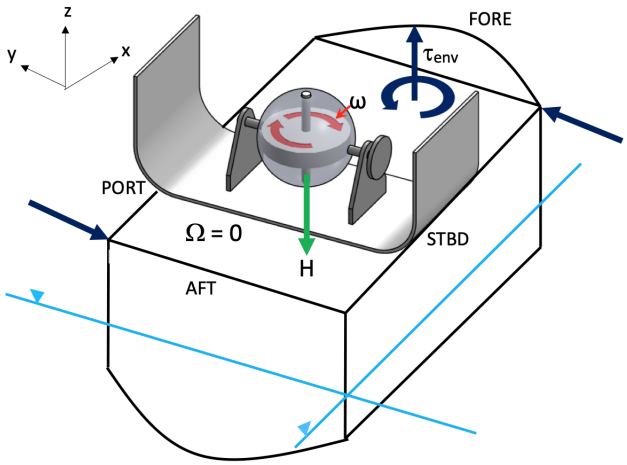

Figure 15: Z-Spin and Y-Fixed flywheel-ship schematic of the induced flywheel moments due to yaw motion

There is no precession, in this case, yielding no flywheel-induced stabilizing moments. There is no H_{sine} term because there is no precession so there is no other flywheel-induced moments. Even if the flywheel to spin counterclockwise, there would still be no precession, so nothing would change. Everything would act normally.

Therefore, there is no need to change anything in the B matrix of the equations of motion

and the matrix would look the same as it started. All the terms in this setup that are affected by a change in yaw remain unaffected.

Final B Matrix As stated in the roll section, $F_{ij} = nHq$. We will factor the constant q out of all the equations for the remainder of this section so now $F_{ij} = nH$. Therefore, $M_{44} = -nH\dot{\phi}$ and $M_{45} = \tau_{prec} = nH\dot{\phi}$ (see active flywheel section for explanation). These moments are moved to the left side of the equation of motion and added to the damping matrix. All following flywheel moments will be referred to $F_{ij} = nH$ and their signs in the Final B_{fly} matrix will be correct for when the B_{fly} matrix is added to the overall B matrix of the ship.

In the following matrix, the top sign in front of a term refers to the sign of the flywheel moment when the flywheel is spinning positive counterclockwise and the bottom sign in front of a term refers to the sign of the flywheel moment when the flywheel is spinning negative clockwise.

Case Z-Y: Z-Spin, Y-Precession

$$B_{fly} = \begin{bmatrix} F_{44}cos(\alpha) & \mp F_{45} & 0 \\ 0 & 0 & 0 \\ \pm F_{64}sin(\alpha) & 0 & 0 \end{bmatrix} \tag{30}$$

6.4 Results & Discussion

This section will discuss the results that were output from the SHIPMO code, mainly, the RAOs of ships with flywheels. Only the first and second flywheel cases, Case Z-Y (spin axis in z-axis, fixed axis in y-axis) and Case Z-X (spin axis in z-axis, fixed axis in x-axis), which were discussed in the first conceptualization section, will be discussed. The other seven flywheel scenarios RAOs are not necessary for this initial analysis but can easily be recreated.

The control case, which is when no flywheels are added to the ship and only numbers 1 and 2 of the source code modification list were applied, was run through the fortran compiler, the RAO output file was exported to an Excel file named "RAO copy.xlsx", and read into a MATLAB file named "Rao_Graph_Updated.m". This MATLAB script produced RAOs of the ship in all six degrees of freedom and these graphs will be what the RAOs of ships with flywheels will be compared to.

For a ship with flywheels, each term of the B matrix, as stated in the source code modification section, will be appended with a F_{ij} term according to the B_{fly} matrices in the theory section. This analysis assumes that the flywheels are outfitted to the ship in an ideal way. Mainly, there is no friction between the bearings of the flywheel support structure, the additional weight, and center of gravity changes are negligible, and the only change in the source code necessary to include flywheels is the additional B_{fly} matrix terms.

Another important assumption is that for this analysis, there are no programmable abilities of the nutation motor to force the flywheel to precess at a designated rate. Active flywheels

with nutation are useful machines but this analysis will only consider precession that is proportional to the rotational rate of the vessel, and not a designated precession rate.

There are a number of variables that can be changed in this analysis: the number of flywheels, the rotational rate of the flywheel, the moment of inertia of the flywheel, or whether all terms of the B_{fly} are included. This analysis will assume that the flywheel described in Table 13 is a standard flywheel to put on a ship so the rotational rate and moment of inertia will not need to change. This leaves the number of flywheels on board and which B_{fly} terms are included to be variable. These will be factored into the SHIPMO runs.

It should also be noted that for ease of analysis, the cosine and sine terms of various terms in the B_{fly} matrices are ignored when put into SHIPMO. The goal is to simply see what happens to the RAOs when flywheel-induced moments are added to the B matrix and cosines and sines will not significantly alter those findings.

The way that this analysis' SHIPMO code is set up, there will be RAOs for all six degrees of freedom, for five different wave angle headings (0 degrees to 180 degrees by increments of 45 degrees), as stated in the SHIPMO.IN section. SHIPMO also follows the same coordinate system as described by Figure 10 so that when the wave angle heading is 90 degrees, the ship will roll positive starboard and stay consistent with the previously described flywheel theory. Also, when there is a wave angle heading from 0 or 180 degrees, the vertical plane motions (sway, roll, and yaw) will have no change for a perfect wave, so there will be no RAOs for those cases.

6.4.1 Case Z-Y

For the Z-Y case, a flywheel is outfitted to a ship with its spin axis pointed in the vertical direction and it has a fixed axis about the y-axis. According to the theory section, when this flywheel is spinning at a high rotational rate ω and undergoes roll, pitch, or yaw motion, it will induce three moments and create a F_{44} and F_{64} term due to roll and a F_{45} term due to pitch. Depending on the direction of spin of the flywheels, the F_{45} and F_{64} terms can change sign. Theoretically, if there are n flywheels on the ship and $n/2$ are spinning in one direction and $n/2$ are spinning in the opposite direction, their induced moments will cancel each other out. The only moment that will always be there will be the F_{44} term.

6.4.2 F44 Term Only

One important consideration is the number of flywheels it takes to significantly alter the seakeeping effects of a ship. Assuming the conditions of the previous paragraph where only the F_{44} term is apparent in this scenario, SHIPMO was run for a case of one flywheel on board, 10 flywheels on board, and 100 flywheels on board. Figure 16, Figure 17 and Figure 18 show how the roll RAO changes with different numbers of flywheels on board for three different wave angle headings. Table 14 then shows the changes in the peak value of the RAO for each number of flywheel run.

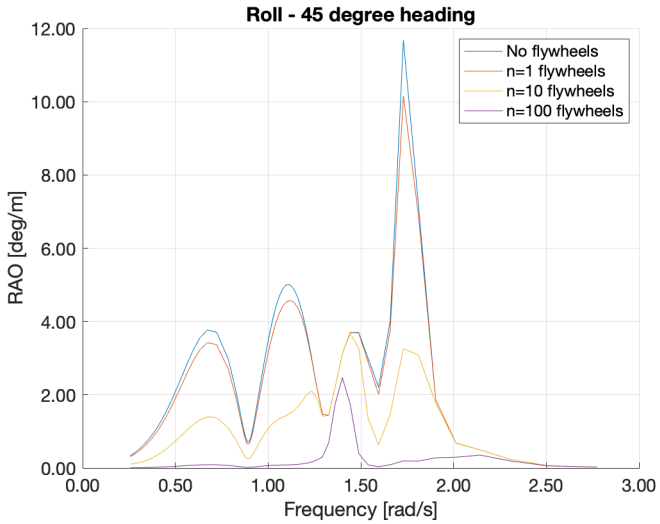

Figure 16: Roll RAO at a 45-degree wave angle heading for three different numbers of flywheels

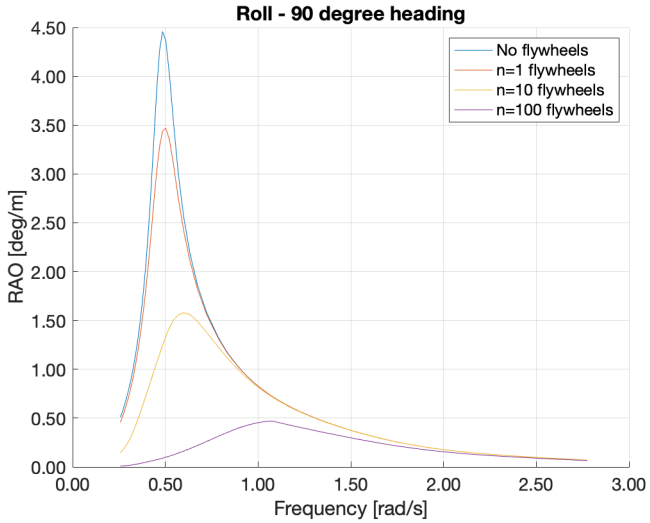

Figure 17: Roll RAO at a 90-degree wave angle heading for three different numbers of flywheels

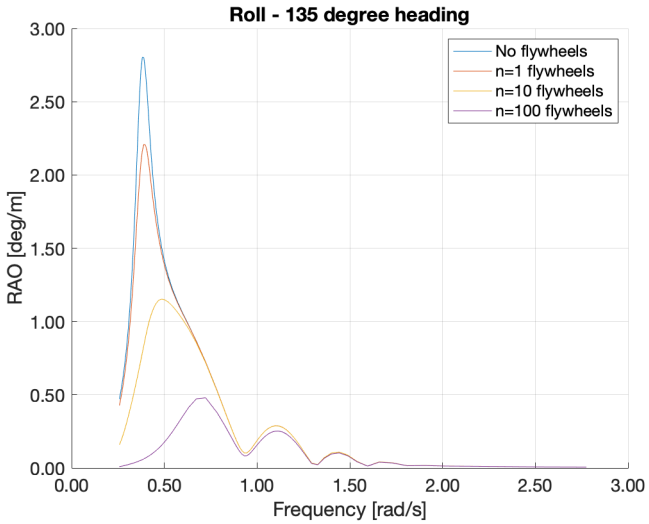

Figure 18: Roll RAO at a 135-degree wave angle heading for three different numbers of flywheels

Table 14: The peak RAO value for each case of a different number of flywheels and the percent decrease from the control run

	Pk	**%**	**Pk**	**%**	**Pk**	**%**
$\beta°$	45		90		135	
n=0	11.7	0.0	4.5	0.0	2.8	0.0
n=1	10.1	13.7	3.5	22.2	2.2	21.4
n=10	3.7	68.4	1.5	66.7	1.15	58.9
n=100	2.5	78.6	0.5	88.9	0.49	82.5

As seen from the figures and the table, the addition of just one flywheel on the ship increases the value of the B_{44} term in the equations of motion, which increases the overall damping of the ship in roll, which decreases roll motion and agrees with the theory. In this simulation, with the given setup and preferences, one flywheel in this orientation decreases the roll motions of the ship by 13.7% for a wave angle heading of 45 degrees, 22.2% for a wave angle heading of 90 degrees, and 21.4% for a wave angle heading of 135 degrees.

As seen in Table 14, the addition of more flywheels decreases the roll motions by even more. This is still under the assumption that in the case of $n = 10$ and $n = 100$ flywheels, there are $n/2$ flywheels that spin in one direction and $n/2$ flywheels that spin in the opposite direction. Also, Table 13 gives the volume and deck area of a flywheel as 20 m^3 and 2.5 m^2 respectively. These values must be taken into consideration when thinking about outfitting a ship with flywheels because even though 100 flywheels might bring the roll motions down more than 80%, there might not be 2,000 m^3 of spare volume or 250 m^2 of deck area available.

However, this analysis' half spinning one way half the other way assumption might not be valid. With this assumption, the flywheel-induced moments of F_{45} and F_{64} should cancel each other out and there should be no change in the RAOs from those terms. SHIPMO does

not agree. With the addition of only the F_{44} term to the B matrix, there is a change in the yaw RAO. The figures below show this phenomenon.

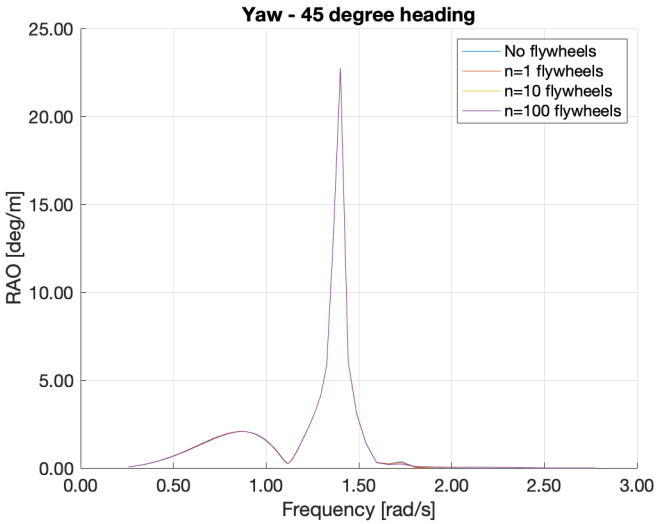

Figure 19: Yaw RAO at a 45-degree wave angle heading for three different numbers of flywheels

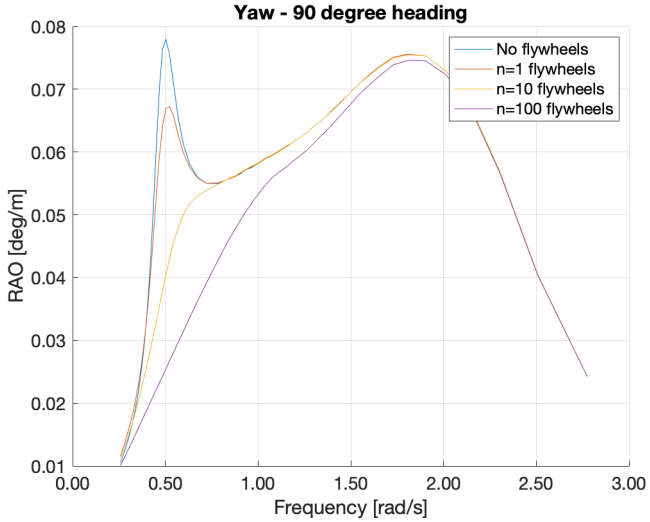

Figure 20: Yaw RAO at a 90-degree wave angle heading for three different numbers of flywheels

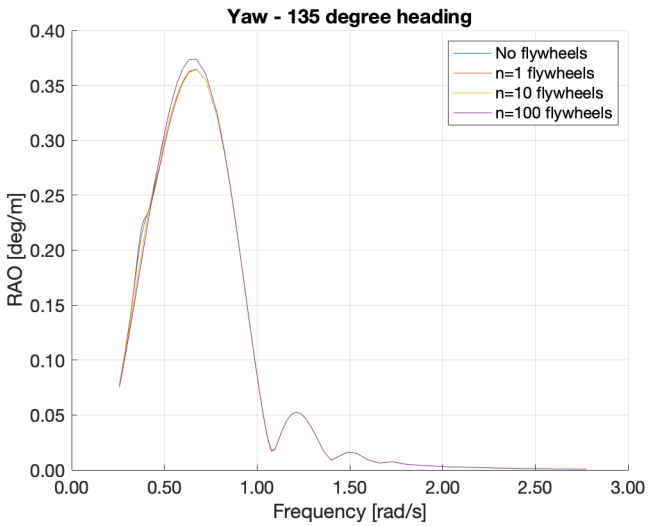

Figure 21: Yaw RAO at a 135-degree wave angle heading for three different numbers of flywheels

As seen from the figures, not all the yaw RAOs remain unchanged when only the B_{44} term is changed. The 45-wave-degree heading is consistent with the theory, but the 90-wave-degree heading yaw RAO decreases as the number of flywheels on board increases. However, it does not change that much, since the peak yaw RAO only reaches about 0.75 degrees per unit wave amplitude. The 135 wave degree heading yaw RAO also changes but not by much. Since the RAOs do not change that much relative to the roll RAOs, this is not that big of a problem, but it is still something to consider for future analysis.

6.4.3 F44 and F45 Terms

Now, the F_{45} term of the B_{fly} matrix of this flywheel orientation will be considered. To reiterate, the F_{45} term is the flywheel-induced moment in roll due to pitch. Based on the theory section, the sign of the F_{45} term is the opposite of the sign of the angular momentum vector of the flywheel. This means that if all the flywheels on board are spinning in the counter-clockwise direction when viewed from above, they will induce a moment on the vessel that will decrease the vessel's damping in roll (4) due to pitch (5). In other words, the vessel will have higher roll motions than the roll RAOs in the F_{44} section, only if all the flywheels are spinning in the same direction. On the other hand, if all the flywheels are spinning clockwise when viewed from above, then their angular momentum vectors would point in the negative z-axis, and the F_{45} term would be positive, which would increase the vessel's damping, and decrease the roll motions of the vessel. The figures below show the relationship of the inclusion of this F_{45} term. Each curve on these figures are for a ship that is outfitted with $n = 10$ flywheels.

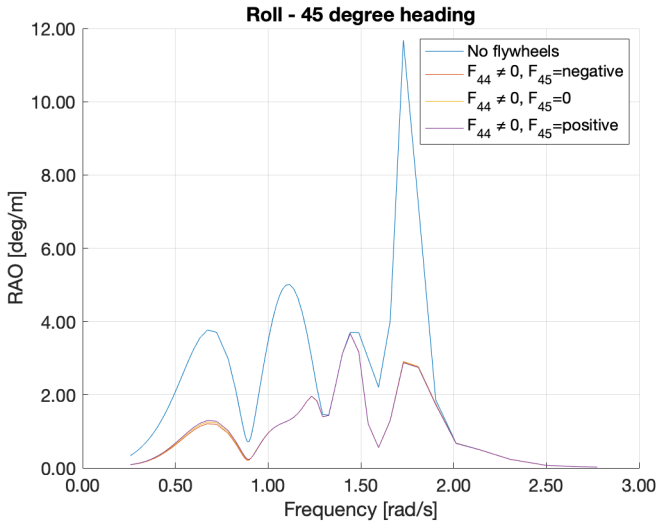

Figure 22: Roll RAO at a 45-degree wave angle heading for either all flywheels spinning one direction (orange), half flywheels spinning one direction and half spinning the other direction (yellow), and all flywheels spinning the opposite direction (purple)

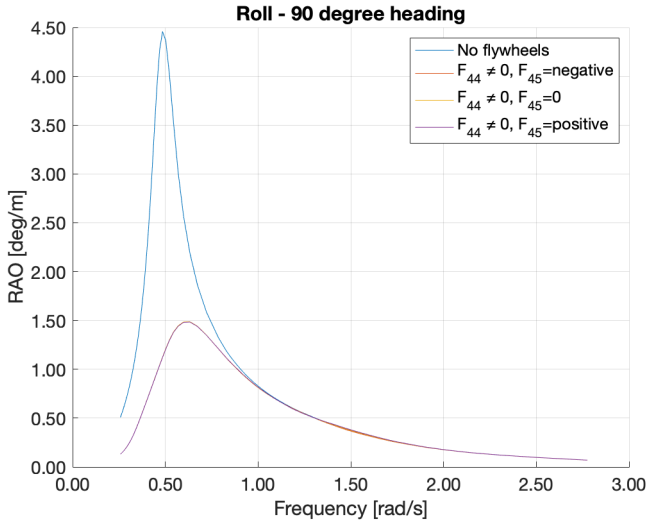

Figure 23: Roll RAO at a 90-degree wave angle heading for either all flywheels spinning one direction (orange), half flywheels spinning one direction and half spinning the other direction (yellow), and all flywheels spinning the opposite direction (purple)

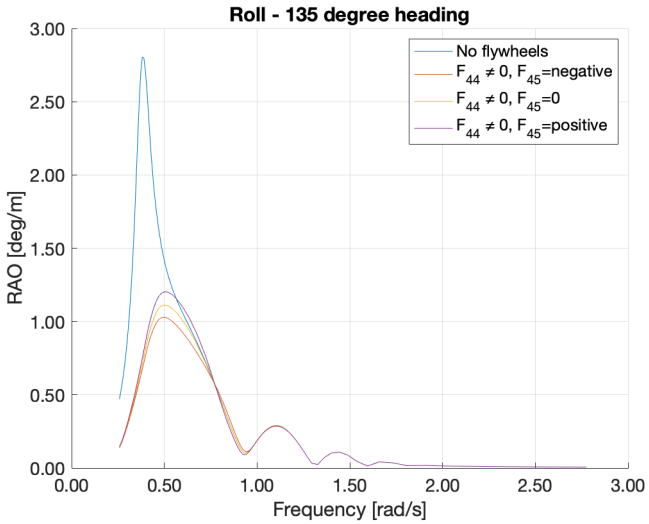

Figure 24: Roll RAO at a 135-degree wave angle heading for either all flywheels spinning one direction (orange), half flywheels spinning one direction and half spinning the other direction (yellow), and all flywheels spinning the opposite direction (purple)

Figure 23 shows the roll RAO at a wave angle heading of 90 degrees. This figure does not show any effect of having a positive or negative F_{45}, which makes sense because a F_{45} term is caused by pitch motion, where there is none of at a 90 degree wave angle heading. With this said, there should be a change in the 45 and 135 wave heading roll RAOs with a F_{45} term, because there should be some magnitude of pitch. This is true, as shown by Figure 22 and Figure 24, but there is not much change. Therefore, it is likely that the ship does not roll as much due to pitch as it does to roll, but there is also a chance that there are discrepancies in the SHIPMO code.

At the 135-degree wave angle heading, as shown by Figure 24, there is more and less roll motion due to a positive and negative F_{45} term, respectively. This is counter-intuitive because the addition of a negative F_{45} term should decrease the ship's damping, which would increase roll motion, but the figure shows that roll motions decrease. The same counter-intuitive reasoning is applied to the positive F_{45} term in the purple curve. However, as the excitation frequency increases, the figure agrees with the theory, but for very small changes. As in, a positive F_{45} term increases damping and decreases roll motions. The cause for this uncertainty in the lower frequencies is unknown for this analysis but is worth looking into for future analyses.

Also, Figure 22 does not change as much as Figure 24, even though they both are at the same magnitude of wave angle headings, just different signs. This might be due to the fore-aft asymmetry of the *USS Ann Arbor*. The one thing that looks to be agreed upon is that roll motions due to pitch are not as great as roll motions due to roll.

6.4.4 F44 and F64 Terms

Making the assumption again that all the flywheels on the ship spin in one direction, there will be a moment in yaw due to roll, or a F_{64} term in the B matrix. For this section, it is also assumed that the F_{45} term is magically set to zero, even though it would not be, so that this section can determine what effect the F_{64} has on the vessel. It should also be noted that ideally, this term would be multiplied by the sine of the precession angle $\sin\alpha$, which, under small angle approximations, is not expected to contribute greatly to the overall motions. Therefore, the F_{64} term is not the most important flywheel-induced moment in this scenario but is still worth analyzing. The following figures show the yaw RAOs of the ship at three different wave angle headings, and each case is set to have 10 flywheels on board.

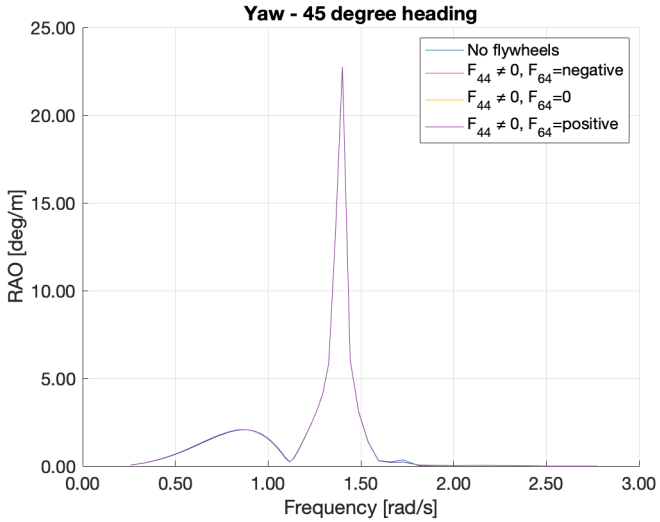

Figure 25: Yaw RAO at a 45 degree wave angle heading for n=10

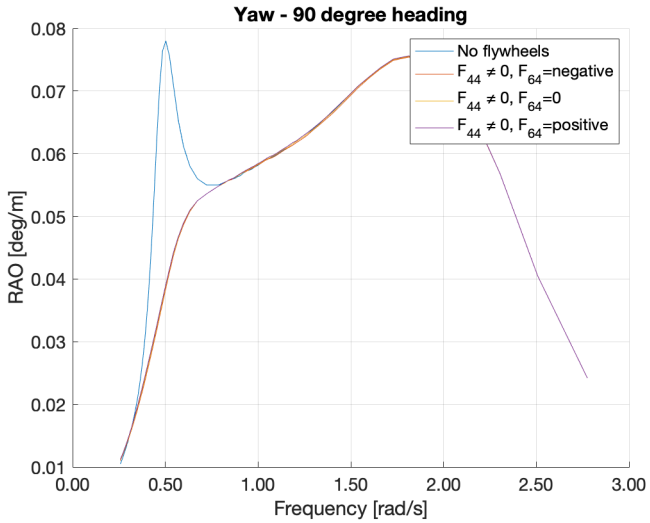

Figure 26: Yaw RAO at a 90 degree wave angle heading for n=10

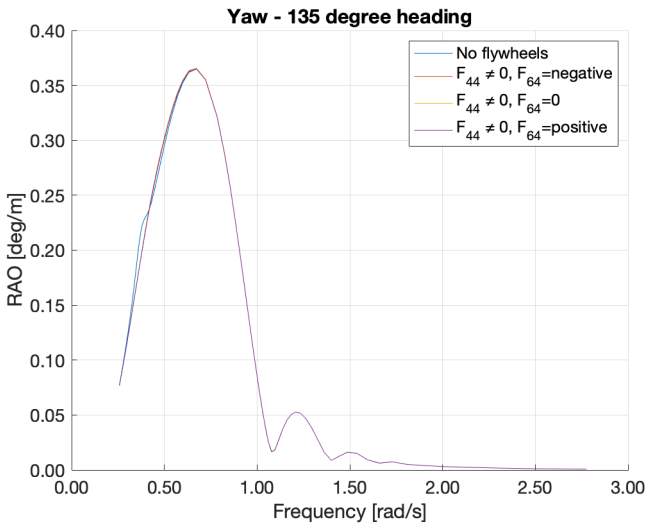

Figure 27: Yaw RAO at a 135 degree wave angle heading for n=10

As seen from these graphs, there seems to be little to no change in the yaw motions of the ship with the addition of a F_{64} term. The yaw RAOs still follow the same form as the yaw RAOs with just the F_{44} term added. The best explanation seems to be that the motions in roll are much more apparent than the motions in yaw, for the same flywheel-induced moment. However, a discrepancy in the SHIPMO code modifications is also possible, or other parts of the code may assume no off-diagonal terms in these matrix positions. This is still being investigated.

6.4.5 Discussion

The main takeaway is that flywheels on a ship in this orientation can reduce roll motions by about 80%, due to the addition of the F_{44} term. The F_{45} and F_{64} terms change sign depending on the direction of the angular momentum of each flywheel. Theoretically, if there are n flywheels on board, $n/2$ are spinning in one direction, and $n/2$ are spinning in the other direction, then their induced moments will cancel each other out. However, that is not necessarily proven in this analysis since the addition of only a F_{44} term changed the yaw RAOs of the ship, even if it was only by a little. Under the assumption that all n flywheels spin in one direction, there would be additional F_{45} and F_{64} terms. The F_{45} term contributes in roll motion due to pitch, but as seen from the figures, it does not contribute that much relatively. The F_{64} term contributes even less and is almost nonexistent. These unpredicted motions are fine for this analysis but would be worth looking into for a future model study.

Assuming the theoretical assumptions of the F_{45} and F_{64} terms, the ship owner can make a trade-off. They have the option of choosing to have $n/2$ flywheels spin one way, and $n/2$ flywheels spin the other way, and there would be no F_{45} or F_{64} terms in the equations of motion. Or, they could choose to have all n flywheels spin in one direction to help motions in one or the other. For example, if all n flywheels were spinning clockwise, then the F_{45} term would be positive, which would increase damping and decrease the roll motions of the vessel. However, the F_{64} term would then be negative, and the yaw motions of the ship

would increase. The same thinking can be applied to the opposite direction of the spin of the flywheel. This trade-off is worth noting theoretically, but it doesn't look like it will significantly contribute to the overall motions of the ship, as shown by the RAOs.

Discrepancies in the SHIPMO code are highly unlikely, as the addition of various B_{fly} terms to the B matrix does what it is supposed to. The "ADMASS" output file lists the added mass, damping, and hydrostatic matrices for various excitation frequencies, and the correct flywheel value was seen in the B_{45} spot. Therefore, it is likely that the RAOs are accurate and are good figures to analyze. The unexpected results are that there are little to no yaw motions of the ship, and that for low frequencies, the addition of a F_{45} term contributes opposite to the theory. However, the change in roll motion due to the F_{45} term does not contribute near as much to roll as the overall F_{44} term. The other explanation is that the given *USS Ann Arbor* characteristics are inadequate or input incorrectly.

7 Demonstrator and Model Tests

The design and construction of the demonstrator FESD were carried out during the fall and winter semesters between the 2021 and 2022 school years, with final testing during the summer of 2022.

7.1 Flywheel Design and Construction

The FESD was designed to fit within the Office of Naval Research Tumblehome (ONRT) ship model. This space limitation resulted in an enclosure that was 8”x8”x8”. A cube was an ideal shape because the FESD could be rotated in different orientations to explore additional effects on pitch and yaw. Those topics are not explored in this paper and are a potential exploration in future work. The frame was built with 20mm 80/20 aluminum framing to be modular and easily assembled or disassembled. For containment, 0.5” thick polycarbonate sheets were cut to size and bolted to the frame. The flywheel was a 12.13 kg machined brass cylinder.

$$I = mr^2$$

The inertia of a flywheel scales exponentially by increasing the radius, however, space constraints restrict the maximum radius. In order to increase the inertia further, the thickness of the flywheel was increased to maximize the mass term.

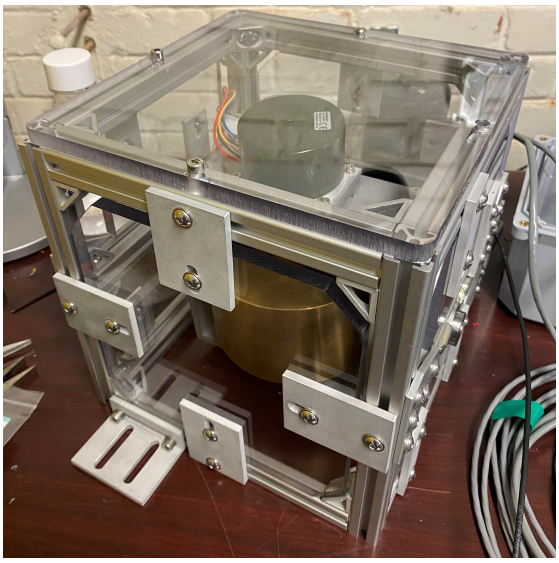

Figure 28: The MHL FESD with containment installed.

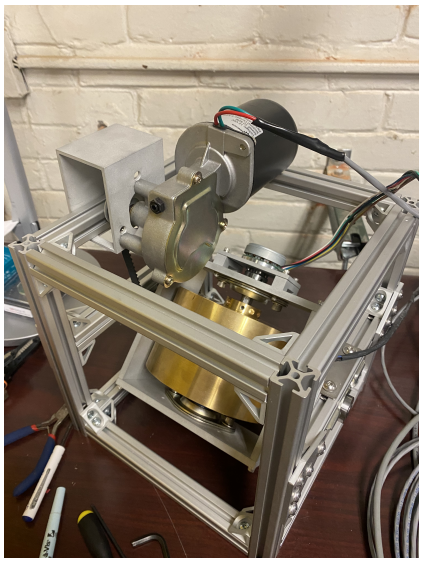

Figure 29: The MHL FESD without polycarbonate containment

To spin the flywheel, a Nanotec Brushless DC pancake motor was used. For precession movement, a worm gear motor was chosen for its high torque at low RPM. The form factor of the pancake motor allowed for a larger range of motion before the precessing assembly was stopped by the polycarbonate containment.

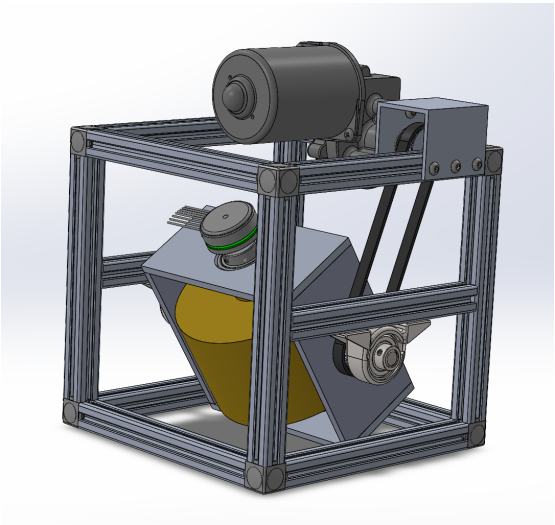

Figure 30: SolidWorks model of the MHL FESD.

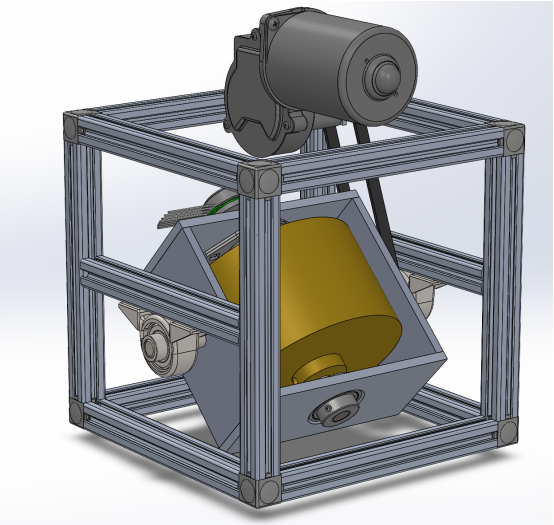

Figure 31: SolidWorks model of the MHL FESD.

An Arduino UNO was used as the microcontroller to run the command script. Serial data from shaft encoders and an Inertial Measurement Unit (IMU) was read into the UNO to provide the roll angle and angle of precession. A PID control loop was used to determine the direction and speed of precession to achieve a roll angle of zero degrees for the model. The coefficients for the proportional, integral, and derivative terms were determined through experimental tuning. While it was hoped to be able to demonstrate energy storage and discharge from the system, the pancake bearings used in the construction of the model proved to be relatively stiff, and as a result, the flywheel would coast to a stop in less than 30 seconds from full RPM (which required the spin motor to be at maximum power to maintain). Finding similar-sized but higher-quality bearings would improve this part of the model significantly.

Table 15: Tested characteristics of MHL FESD.

Parameter	**Value**	**Units**
Maximum Spin Speed	2100	RPM
Maximum Precession Speed	7.51	RPM
Flywheel Moment of Inertia	0.022	kgm^2
Maximum Moment Generated	3.80	Nm
Voltage at Maximum Spin Speed	24.0	V
Amperage at Maximum Spin Speed	3.79	A

7.2 Model vessel

The FESD was mounted to the midship of a 1:49 scale model Office of Naval Research Tumblehome (ONRT) ship. The ONRT is a publicly available hull for research. The Tumblehome

is designed as a modern surface combatant. The use of 80/20 framing for the FESD made it easier to mount to large optical breadboards installed on the model.

Table 16: Characteristics of ONR Tumblehome model.

Parameter	**Value**	**Units**
Length of Waterline, L_{WL}	3.147	m
Maximum Beam of Waterline, B_{WL}	0.384	m
Depth, D	0.266	m
Draft, T	0.112	m
Displacement, ∇	72.6	kg
Wetted Surface Area, S_0	1.5	m^2
Block Coefficient, Cb	0.535	
Longitudinal Center of Buoyancy, LCB	1.625	m
Vertical Center of Gravity, VCG	0.156	m
Metacentric Height, GM	0.0422	m

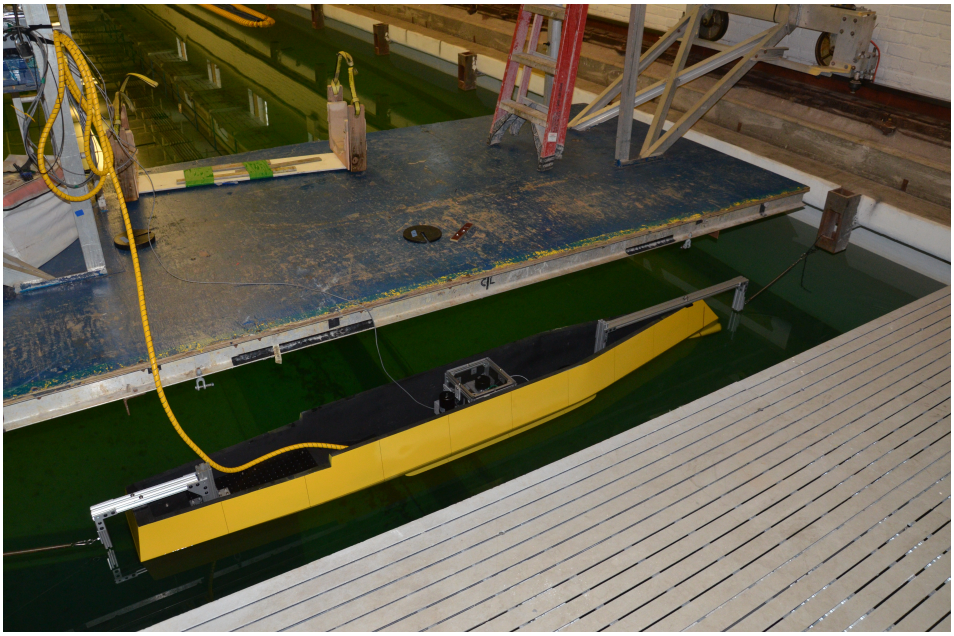

Figure 32: The ONRT model stationed in the wave tank of the University of Michigan Marine Hydrodynamics Laboratory

Tumblehome designs are more susceptible to roll at higher drafts due to the decreasing amount of volume once the section above the waterline is immersed. It was selected for this project due to its susceptibility to roll, and extensive recent research from other academic institutions [17].

7.3 Test Program and Results

In order to follow International Towing Tank Conference (ITTC) guidelines on softly restraining a model during roll decay tests, the roll natural frequency of the model needed to be determined. A rough estimate of 0.966s was found through

$$\omega_{4n} = \sqrt{\frac{mg\bar{GM}}{1.25I_4}} \tag{31}$$

Where $\bar{GM}$ is the metacentric height of the vessel, and I_4 is the roll moment of inertia.

In order to softly restrain the vessel from drifting down the tank, springs were chosen with a natural period one order of magnitude larger than the model's natural roll period [4]. The ONRT was restrained beam-to-waves at the halfway point of the University of Michigan Marine Hydrodynamics Laboratories' 109m towing tank. Using the natural roll period as a starting point, frequencies and amplitude were modified until, through visual inspection, the ONRT was undergoing large roll motions without the potential of capsizing. This resulted in a 0.938 Hz frequency and 2cm amplitude wave. A 50-second wave set was produced per test, which included a ten-second ramp-up and wind-down.

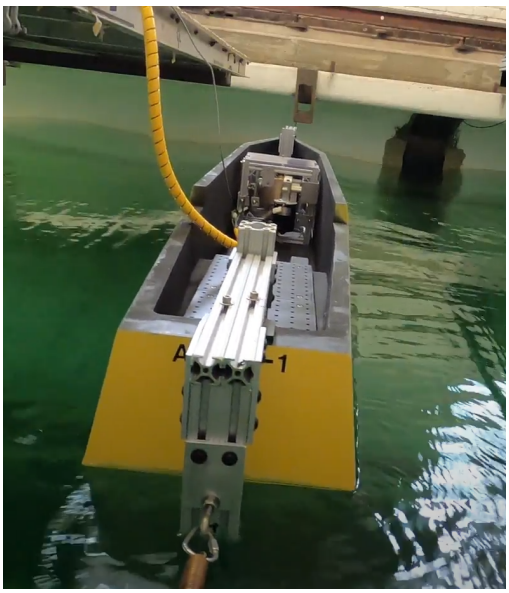

Figure 33: Actively controlled FESD mounted on ONR Tumblehome (Wave Crest)

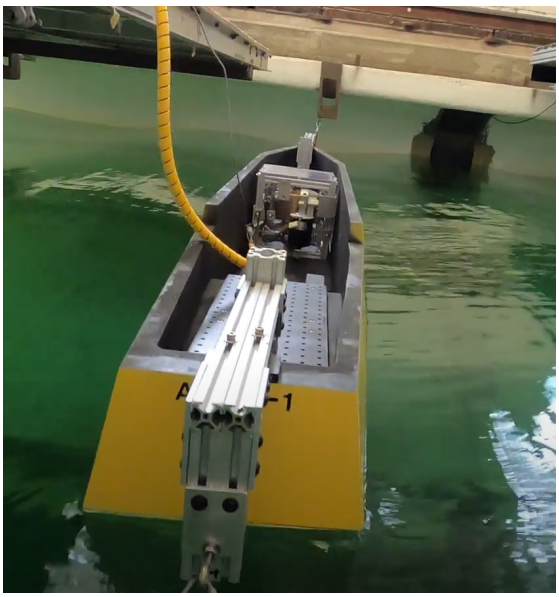

Figure 34: Actively controlled FESD mounted on ONR Tumblehome (Wave Trough)

Three modes of the FESD were tested. To determine the wave set and to provide a baseline against different wave parameters, the flywheel was first shut off to allow the model to roll

freely. The second mode was active stabilization, where the microcontroller read the degree of roll from the IMU unit and powered the precession motor to properly counter the roll. The last mode was passive stabilization, where the precession belt was removed. This allowed the flywheel to freely precess to counter roll. In all three modes, the IMU that was on the hull for active stabilization recorded roll data for comparisons.

In the condition where the flywheel was shut off, the model experienced peak roll motions of 11.34 degrees. With the model being actively stabilized, the amplitude of the roll was reduced by 84.21% to 1.79 degrees. This reduction in roll can be seen in Figure 35. . Interestingly,

passive stabilization reduces roll further than the actively stabilized mode. However, without a control scheme, waves can roll the vessel, and the flywheel will attempt to hold that angle. This can be seen in Figure 35 where the passive mode maintains a roll of 2 degrees in the second half of the test.

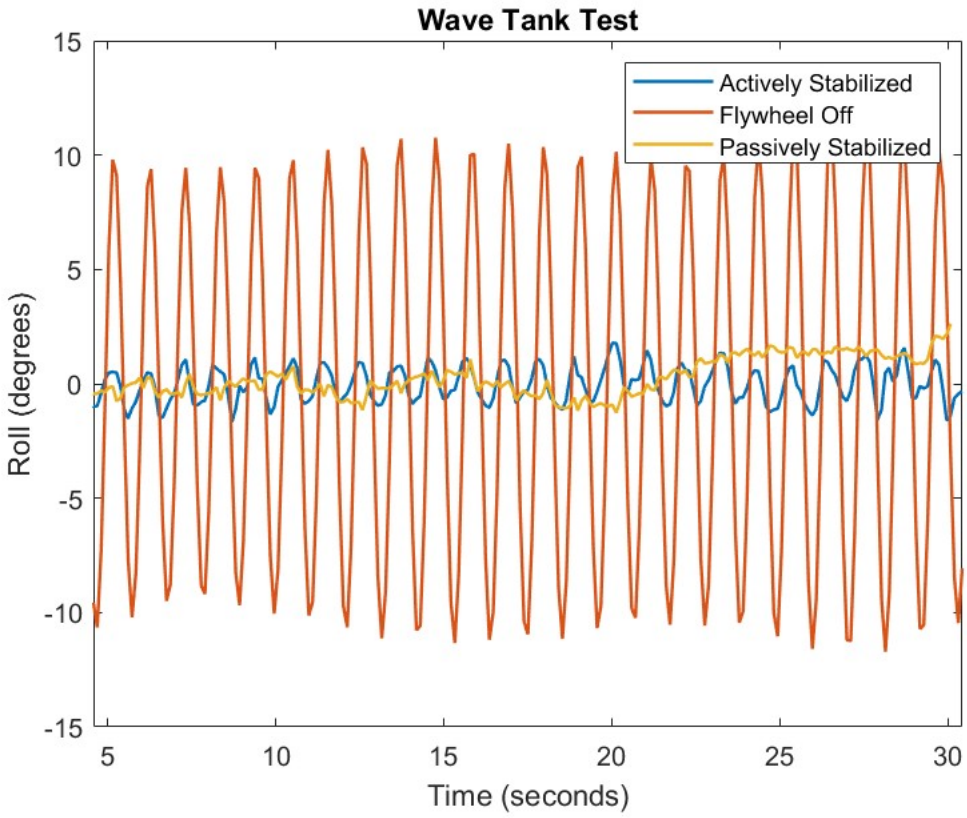

Figure 35: Comparison of roll between round 28 (flywheel off), round 27 (FESD actively stabilized at 2100 RPM), and round 38 (FESD passively stabilized).

By taking the maximum rate of precession from the experimental data, the maximum moment generated by the flywheel was determined. This moment resulted in roughly 3.80 Nm based on the characteristics seen in Table 15.

Table 17: Wave tank test parameters for active stabilization.

Parameter	Value	Units
Spin Speed	2100	RPM
Precession Speed	7.51	RPM
Moment of Inertia	0.022	kgm^2
Moment Generated	3.80	Nm

According to the data presented in Figure 35, the passive stabilization produced a similar response to the active stabilization with a much more gradual roll correction. When met with shock loads, the passive stabilization had longer response times than the tuned active stabilization control. This is further emphasized by the comparison in Figure 36.

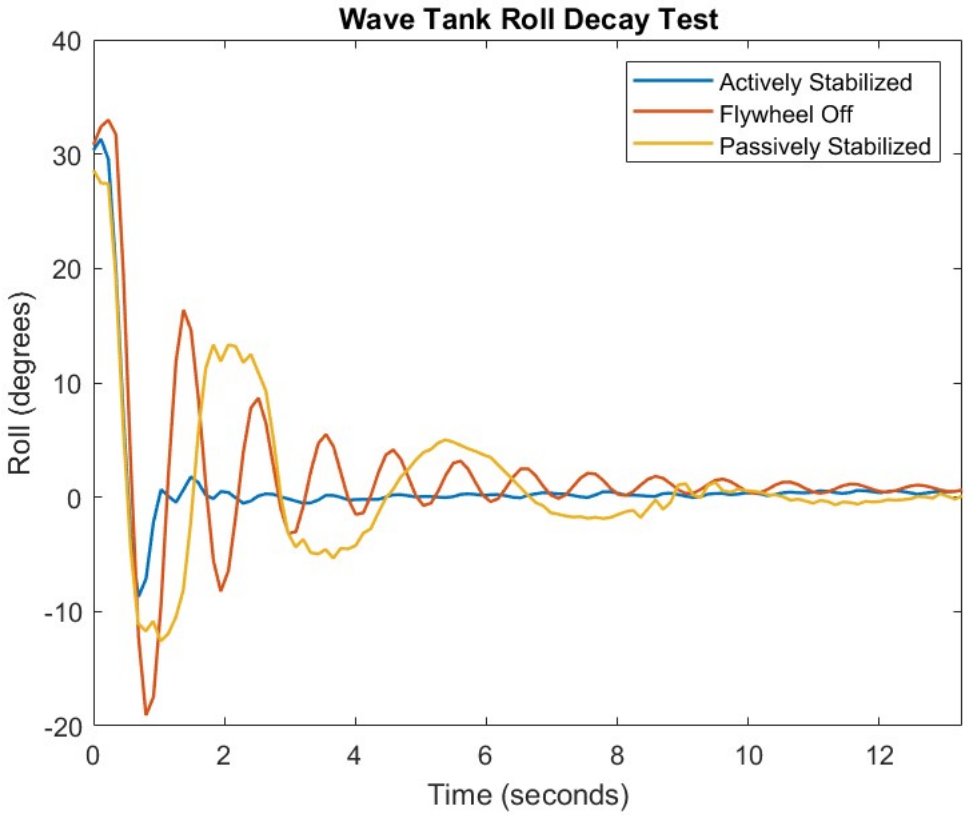

Figure 36: Comparison of roll decay between no stabilization, passive, and active stabilization at 2100 RPM.

The roll decay tests were performed by releasing the model from an angle of 30 degrees in still water. This is where the active stabilization shows its performance benefits over the passive and unstabilized conditions. The active stabilization responds to the change in roll within 2 seconds, where the other conditions still experience light roll motions 10 seconds after release.

Videos showing both the wave and roll decay tests can be found on the MHL youtube channel.[20] [21]

7.4 Extrapolation to full scale

As with all model testing, extrapolation to full scale provides a benchmark for feasibility. In order to replicate these results for a full-scale naval vessel built on the ONRT hullform, a scale factor of the length ratio to the fourth power was used to preserve Froude scaling. A similar scaling procedure is found in reference [12], which lists the factors used to extrapolate model experiments. The scenario selected for scaling is directed at recreating the 84.21% roll reduction from the model experiment. The moment generated by the demonstrator from the wave tank test 27 was used. This is the blue roll response as seen in Figure 35.

Table 18: Moment extrapolation to full scale.

Parameter	**Value**	**Units**
Model Length	3.147	m
Full Scale Length	154	m
Length Ratio (λ)	48.93	
Froude Scale Factor for Moment (Nm)	λ^4	
Froude Scale Factor for Speed (Hz)	$\lambda^(- 0.5)$	
Model Moment	3.80	Nm
Full Scale Moment	21811.44	kNm

As stated previously, the flywheel was able to contribute a moment of 3.80 Nm, which resulted in a full-scale moment of 21881.44 kNm when multiplied by λ^4. In order to determine the feasibility of these results, the performance characteristics of the ALPS FESD from Section 4.1 was used as a benchmark. Using the reported maximum spin speed and moment of inertia for the ALPS FESD, along with the extrapolated full-scale moment, the required precession speed of 340.86 RPM was calculated.

Table 19: Full scale parameters for ALPS flywheel that achieve extrapolated results.

Parameter	**Value**	**Units**
Spin Speed	15000	RPM
Precession Speed	340.86	RPM
Moment of Inertia	389	kgm^2
Moment Generated	21811.44	kNm

Table 19 assumes a single flywheel which will provide the least amount of redesign for installation as discussed in Section 4.1. This puts more reliance on a single FESD which reduces the redundancy in comparison to other configurations. However, the required precession speed is very high, and may be difficult to achieve in practice as this speed would need to be reached once per wave cycle, requiring high acceleration. However, the moment produced is proportional to the precession speed, so by controlling three flywheels, the required speed

could be cut by a third. If one FESD is able to sufficiently provide desirable stabilization and energy storage needs, then increasing the number of FESDs can disperse the load across a bank which improves system resiliency.

With tandem moment control systems, lower operating speeds per FESD can increase the life cycle of rotating components. Arrangements are only limited by the space and weight requirements for the vessel and their compatibility with the parameters in Table 6.

8 Conclusions

FESD offer a range of benefits and challenges for naval vessels. In this initial review of FESD, it seems clear that the benefits outweigh the challenges. Modern, high-speed FESD are unlikely to produce problematic responses when performing charge/discharge cycles. For a frigate-sized vessel, the weight impacts of FESD are perhaps most notable on the design, with a much smaller impact on the arrangeable area. This proved true over a range of possible FESD use cases, ranging from high-power loads to replacing standby generators. While retrofitting FESD into existing vessels may be challenging owing to the high outfit density of naval vessels, clean-sheet designs of new vessels with FESD seem well within reach from an overall design perspective. However, maintenance needs, as well as any safety concerns with rotating masses in combat situations, were not reviewed in this work.

FESD may also be useful on smaller vessels. Here, the primary advantage is reliable energy storage that may reduce the running hours or number of starts of diesel generators. Additionally, as shown later, the seakeeping benefits of FESD are significant, and for smaller vessels, especially when loitering (at speeds where fin stabilizers are less effective), FESD look very attractive. An initial design space exploration program was set up using parametric models to explore the impact of FESD on the overall vessel design. Here, unlike the Frigate study, significant increases in mass (and vessel size) were required if the number of engine starts was to be dramatically reduced. However, the resulting Pareto front between engine starts and mass was very steep, indicating that halving the number of engine starts may be possible for smaller (<10%) changes in vessel mass.

While charge/discharge cycles were not deemed critical for impacting ship motions, the gyroscopic moments associated with FESD were shown to be much larger. A series of modifications to a linear strip theory seakeeping code was made by supplementing both the damping matrix and the forcing matrix (for controlled precessions configurations) with new terms related to the moments from the FESD. By theory, these appeared to be large enough to impact the vessel's overall motion and resulted in visually different RAOs.

To confirm the theoretical predictions, a scale demonstrator was constructed using a controllable flywheel and a modern tumblehome naval ship design. The FESD could be mounted fixed, free to passively precess, or in force precession to generate roll-countering moments. The model was tested in regular waves near the natural frequency of the model to generate large roll motions. Additionally, roll decay tests were conducted. Overall, the actively controlled flywheel reduced motions by almost 90%. Interestingly, the passively controlled flywheel performed almost as well, but in this configuration, the model had a tendency to "hang" at non-zero roll angles for several wave encounters. Overall, the motion tests were highly encouraging, and expanding the forces to full scale indicated that it may be practical to force similar moments on full-scale vessels, though it may take multiple FESD.

This project was significantly impacted by COVID, which resulted in the loss of much experimental time. Additionally, the Co-PI directing the experimental and hydrodynamic side of the program left the University during COVID. This required a new cohort of students

to take over the model construction and testing. Despite these challenges, eight students had significant (often 12-18 month long) involvement in the project, meeting the original objective of introducing FESD to a cohort of undergraduate and graduate students.

Future exploration of FESD is highly recommended. The ability to either actively or passively control FESD should be explored by researchers working on the design of these devices. Additionally, the "hanging" behavior in the passive model (which would be easiest to achieve in the full-scale FESD) should be further explored. This may be related to the bearing friction in the scale model or maybe a physical phenomenon that needs to be accounted for in design. Further testing of the model in irregular seas and a comparison of the motion reduction with operability criteria would also be beneficial. The reliability and synthesis model used for the MUSV-sized vessel study could also be further refined. As machinery reliability continues to be a struggle for crewless platforms, high-reliability FESD may be a useful way forward to improve the operability of these platforms. Finally, the linearized seakeeping model developed here could be easily transposed into a non-linear time-domain model in a code like the Navy's LAMP program, which would allow a more accurate impact of FESD on ship motions, both positive and negative, to be considered.

References

[1] Robert F. Beck and Armin W. Troesch. *Documentation and Users Manual for the Computer Program SHIPMO.BM*. Ann Arbor, Michigan, Sept. 1989.

[2] Thomas Wightman Chalmers and Thomas Wightman Chalmers. *The automatic stabilisation of ships*. London: Chapman & Hall, ltd., 1931.

[3] *Energy Density - Wikipedia*. URL: https://en.wikipedia.org/wiki/Energy_density.

[4] *Estimation of Roll Damping*. Stability in Waves Comittee. International Towing Tank Comittee. URL: https://www.ittc.info/media/9759/75-02-07-045.pdf.

[5] Larrie D. Ferreiro and Mark H. Stonehouse. "A Comparative Study of US and UK Frigate Design". In: *SNAME Transactions* 99 (Nov. 1991).

[6] GlobalSecurity.org. *Medium Unmanned Surface Vessel (MUSV)*. URL: https://www.globalsecurity.org/military/systems/ship/musv.htm.

[7] James Gose et al. *Exploration of Ship-Level Impacts of Flywheel Energy Storage Devices*.

[8] Izvor Grubisic and Ermina Begovic. "Reliability of attribute prediction in small craft concept design". In: 1 (Jan. 2012), pp. 439–448. DOI: 10.1201/b11810-69.

[9] Izvor Grubisic and Ermina Begovic. "Upgrading weight prediction in small craft concept design". In: (Oct. 2009).

[10] Robert E. Hebner, John D. Herbst, and Angelo L. Gattozzi. "Pulsed Power Loads Support and Efficiency Improvement on Navy Ships". In: *Naval Engineers Journal* 122.4 (2010), pp. 23–32. DOI: 10.1111/j.1559-3584.2010.00277.x.

[11] J. D. Herbst et al. "Rotating Machine Technologies for Integration of Pulsed and High Power Loads in Naval Electric Power Systems". en. In: *IEEE ESTS 2013*. IEEE, Apr. 2013. (Visited on 12/09/2017).

[12] Mohammed(Shameem) Islam, Fatima Jahra, and Scott Hiscock. "Data analysis methodologies for hydrodynamic experiments in waves". In: *Journal of Naval Architecture and Marine Engineering* 13 (June 2016), p. 1. DOI: 10.3329/jname.v13i1.25347.

[13] *Lec 24: Rolling Motion, Gyroscopes | 8.01 Classical Mechanics, Fall 1999 (Walter Lewin)*. URL: https://www.youtube.com/watch?v=N92FYHHT1qM (visited on 02/18/2020).

[14] J. Mcgroarty et al. "Flywheel energy storage system for electric start and an all-electric ship". In: *IEEE Electric Ship Technologies Symposium, 2005.* (2005). DOI: 10.1109/ests.2005.1524706.

[15] J. L. Meriam and L. G. Kraige. *Dynamics*. 7th ed. Engineering mechanics v. 2. OCLC: ocn299699736. Hoboken, NJ: Wiley, 2012. ISBN: 978-0-470-61481-5.

[16] Anthony F. Molland, Stephen R. Turnock, and Dominic A. Hudson. *Ship Resistance and Propulsion: Practical Estimation of Propulsive Power*. Cambridge University Press, 2011. DOI: 10.1017/CBO9780511974113.

[17] *ONR Tumblehome Ship (ONRT)*. URL: https://www.w2022.nl/onr-tumblehome-ship-onrt/. (accessed: 07.07.2022).

[18] Tristan Perez and Paul D. Steinmann. "Analysis of Ship Roll Gyrostabiliser Control". en. In: *IFAC Proceedings Volumes*. 8th IFAC Conference on Manoeuvring and Control of Marine Craft 42.18 (Jan. 2009), pp. 310–315. ISSN: 1474-6670. DOI: 10.3182/20090916-3-BR-3001.0007. URL: http://www.sciencedirect.com/science/article/pii/S1474667016319139 (visited on 02/22/2020).

[19] *RB48V300 48V 300Ah LiFePO4 Battery*. URL: https://relionbattery.com/products/lithium/rb48v300.

[20] *Roll Decay Video*. URL: https://www.youtube.com/watch?v=GAAd6XO8Ddw&t=51s.

[21] *Roll Motion Video*. URL: https://www.youtube.com/watch?v=kMepSqWONmo.

[22] Paul Steinmann. *How Gyros Create Stabilizing Torque*. URL: http://veemgyro.com/wp-content/uploads/2015/11/White_Paper_1403-How_Gyros_Create_Stabilizing-Torque.pdf (visited on 02/18/2020).

[23] Muhammad Talha, Furqan Asghar, and Sung Ho Kim. "Design of Fuzzy Tuned PID Controller for Anti Rolling Gyro (ARG) Stabilizer in Ships". en. In: *International Journal of Fuzzy Logic and Intelligent Systems* 17.3 (Sept. 2017). Publisher: Korean Institute of Intelligent Systems, pp. 210–220. ISSN: 1598-2645. DOI: 10.5391/IJFIS.2017.17.3.210. URL: http://www.ijfis.org/journal/view.html?doi=10.5391/IJFIS.2017.17.3.210 (visited on 02/22/2020).

[24] R F Thelen, J D Herbst, and M T Caprio. "A 2MW Flywheel for Hybrid Locomotive Power". In: *2003 IEEE 58th Vehicular Technology Conference*. Institute of Electrical and Electronics Engineers, 2003. URL: https://ieeexplore.ieee.org/abstract/document/1286244.

[25] Joseph Van Houten. "Predicting the Stability and Seakeeping Impacts of Flywheel Energy Storage Technology on United States Vessels". PhD thesis. University of Michigan, May 2019.

[26] *Wärtsilä Solutions for Marine and Oil and Gas Markets*. URL: `https://www.wartsila.com/docs/default-source/marine-documents/segment/brochure-marine-solutions.pdf`.

A Energy Storage Comparison

This section includes calculations done to explore relative energy density and specific energy of power sources. This shows that for large energy requirements, flywheel energy storage devices fall very short of traditional diesel fuel and generators.

A.1 ALPS FESD

Table 20: Summary of ALPS Flywheel specifications [24]

Parameter	**Value**
Rated Power	2 MW
Deliverable Energy	360 MJ
Overall Mass	18 t
Overall Volume	20 m^3

$$360\,\text{MJ}\ \textbf{Specific Energy:}\ e_{fw} = \frac{360\,\text{MJ}}{18\,\text{t}} = 20\,000\,\tfrac{\text{J}}{\text{kg}}$$

$$360\,\text{MJ}\ \textbf{Energy Density:}\ \rho_{fw} = \frac{360\,\text{MJ}}{20\,\text{m}^3} = 18\,\text{MJ/m}^3$$

$$3600\,\text{MJ}\ \textbf{Specific Energy:}\ e_{fw} = \frac{3600\,\text{MJ}}{180\,\text{t}} = 20\,000\,\tfrac{\text{J}}{\text{kg}}$$

$$3600\,\text{MJ}\ \textbf{Energy Density:}\ \rho_{fw} = \frac{3600\,\text{MJ}}{200\,\text{m}^3} = 18\,\text{MJ/m}^3$$

A.2 Medium-Speed Diesel Generators

Based on the Wartsila 16V14 medium-speed diesel generator set. Diesel fuel has a specific energy of $e_{diesel} = 45\,600\,000\,\frac{\text{J}}{\text{kg}}$, and energy density of $\rho_{diesel} = 38\,600\,\text{MJ/m}^3$ [3].

$$360\,\text{MJ}\ \textbf{Specific Energy:}\ e_{fw} = \frac{360\,\text{MJ}}{15.01\,\text{t}} = 23\,987\,\tfrac{\text{J}}{\text{kg}}$$

$$360\,\text{MJ}\ \textbf{Energy Density:}\ \rho_{fw} = \frac{360\,\text{MJ}}{22.68\,\text{m}^3} = 15.87\,\text{MJ/m}^3$$

$$3600\,\text{MJ}\ \textbf{Specific Energy:}\ e_{fw} = \frac{3600\,\text{MJ}}{15.1\,\text{t}} = 238\,743\,\tfrac{\text{J}}{\text{kg}}$$

Table 21: Summary of generator and fuel specifications [26]

Parameter	Generator	Diesel Fuel	Total
Rated Power	1 MW	-	2 MW
Deliverable Energy	-	360 MJ	360 MJ
Overall Mass	7.5 t	0.01 t	15.01 t
Overall Volume	11.33 m^3	0.01 m^3	22.68 m^3

$$3600\,\text{MJ}\ \textbf{Energy Density:}\ \rho_{fw} = \frac{3600\,\text{MJ}}{22.76\,\text{m}^3} = 158.2\,\text{MJ/m}^3$$

A.3 Lithium Batteries

Based on Relion RB48V300 48 volt 300 amp − hour LiFePO4 Battery.

Table 22: Summary of RB48V300 Lithium Battery specifications [19]

Parameter	Single Battery	Total
Rated Power	9.6 kW	62.5 kW
Deliverable Energy	55.3 MJ	360 MJ
Overall Mass	0.176 t	1.15 t
Overall Volume	0.146 m^3	0.953 m^3

$$360\,\text{MJ}\ \textbf{Specific Energy:}\ e_{fw} = \frac{360\,\text{MJ}}{1.15\,\text{t}} = 314\,182\,\tfrac{\text{J}}{\text{kg}}$$

$$360\,\text{MJ}\ \textbf{Energy Density:}\ \rho_{fw} = \frac{360\,\text{MJ}}{0.953\,\text{m}^3} = 377.8\,\text{MJ/m}^3$$

$$3600\,\text{MJ}\ \textbf{Specific Energy:}\ e_{fw} = \frac{3600\,\text{MJ}}{11.5\,\text{t}} = 314\,182\,\tfrac{\text{J}}{\text{kg}}$$

$$3600\,\text{MJ}\ \textbf{Energy Density:}\ \rho_{fw} = \frac{3600\,\text{MJ}}{9.53\,\text{m}^3} = 377.8\,\text{MJ/m}^3$$

A.4 Summary

As seen in the comparison between the ALPS FESD and medium-speed diesel generator, the specific energy and energy density of the two are roughly equal at 360 MJ of energy. However, the ALPS flywheel has constant energy density (assuming an integer multiple of its capacity). In contrast, the medium-speed diesel generator has much higher specific energy and energy density for larger capacities. This is due to the extremely high specific energy and energy density of diesel fuel.

The capacity of one ALPS FESD, 360 MJ equates to 100 kW of power for one hour or 5 kW of power for twenty hours. This suggests that in regimes where the power demand for the vessel is low, the FESD could provide power at a comparable expense in terms of space and

weight. Additionally, the FESD can be charged and discharged an infinite number of times.

A study of the effectiveness of lithium batteries is potentially warranted as well, as the energy density and specific energy of lithium batteries is very high despite relatively low power ratings. Batteries can provide some of the same benefits as FESDs, and could provide an interesting comparison.

B SHIPMO.IN

This appendix will describe the formatting of the input file to the SHIPMO program. This appendix was derived from the SHIPMO User Manual [1] to be rewritten in a way that makes a little more sense to the user.
The SHIPMO.IN file is the input file to make changes to, depending on what calculations are desired. Each step, or card #, in the manual, corresponds to that section, or line, in the SHIPMO.IN file.

1. The first section is very open-ended and allows the user to create a name for the ship or project that will be calculated.

2. The second section takes 15 inputs ranging from IA to NPAC for the user to determine and input to the SHIPMO.IN file. The inputs can be determined from the manual (See page 63-64). The inputs range from the unit system, the wave spectrum, or the number of degrees of freedom.

3. The third section takes in six inputs but more related to the physics of the simulation, such as the ship length and water depth.

4. The fourth section takes in three inputs related to the bilge keel.

5. The fifth section is to be included only if IL=1, where there is a shift in the input offset axis, and the three inputs to the fifth section quantify that shift.

6. When IL=0, the sixth section describes the shape of each station. It has four inputs, which are the number of input points, or y-z coordinates, for each station number. The maximum number of stations is 21 and there must be a station at x=0 (midships). It also takes in the x-location of the station, the bilge radius, and whether it has a lid or not on the station to prevent irregular frequencies. The following 15 lines of each station number (input points) describe the y-axis and z-axis location of the station (how the cross section looks). The first input point is at the keel and works up. For twin-hulled bodies, the first point starts at the inboard most point and works outboard. There are usually 21 stations for each simulation.

7. After all the station geometries are set, the seventh section describes the total VCG positive above waterline and the roll radius of gyration.

8. The eighth section relates to the longitudinal weight distribution. The first input is the LCG positive of midship, the second input is the pitch radius of gyration about the y-axis and also the yaw radius of gyration about the z-axis. The third input is the polar moment of inertia I45.

9. The ninth section is to be used if IN is not 0 and it relates to the surge viscous resistance.

10. The tenth section is to be used if NPAC is not zero and relates to motion points.

11. The eleventh section takes in seven inputs. The wave amplitude, the lowest wavelength or frequency, the biggest wavelength or frequency, the increment in wavelength or frequency (ft or m for regular waves, or rad/s for irregular waves and the maximum number is 51), the minimum and maximum ship speed, and the increment in ship speed.

12. The twelfth section relates to the empirical roll damping and is to be included if IH=0 and IE>0.

13. The thirteenth element takes three inputs for wave angle headings: the initial wave angle or wind direction, the final wave angle in degrees, and the increment in wave angle (maximum number is 25 and if short crested, use the wind direction).

14. The fourteenth section is to be included if ID>=1 and is used to describe the irregular wave spectrum.

All the units for each variable should be assumed as the conventional units based on the unit setting the user selected. More information can be found in the SHIPMO User Manual [1].

C Source Code: shipmo.bm.v1.2.f

This section of the appendix will list the descriptions of what each subroutine in the SHIPMO source code does. Again, a more detailed description can be found in the SHIPMO User Manual [1]. There are some subroutines where their common blocks had flywheel terms that were added. Those changes will be signified by the phrase "Flywheel variables added" in italics at the end of the respective subroutine descriptions. These descriptions were taken from Joey's "SHIPMO Line-by-Line" document in the Flywheel Google Drive.

Lines 1-37: Initial Comments This section is the title of the code and how to run it.

Lines 38-278: First Part This is the main part of the code that goes through the flowchart but calls subroutines and functions located below it.

Lines 279-819: Subroutine PRELMB PRELMB reads in the ship data and checks the hydrostatics

Lines 820-875: Subroutine FILLMX This subroutine fills the mass and hydrostatic matrices. Lines 837-842 initialize the mass and C matrices. Lines 864-870 fill the hydrostatic restoring force coefficients.

Line 876-970: Subroutine WTCURV Compute weight, centers of gravity, and roll and pitch radii of gyration of ship from a weight curve

Line 971-1017: Subroutine ZCGINT Compute integral for weight, moment, vertical center of gravity using a linear fit

Line 1018-1067: Subroutine SAREA Compute the area and centroid of section

Line 1068-1123: Subroutine XWTS Compute the weights for Trap and TrapX integration

Line 1124-1180: Subroutine XWTSCV Compute the weights for TrapCV and TrapXC integration

Line 1181-1202: Function TRAPX Integrate a function y from x to L/2

Line 1203-1224: Complex Function CTRAPX Integrate a complex function y from x to L/2

Line 1225-1241: Function TRAPCV Integrate the weight curve over the ship length

Line 1242-1263: Function TRAPXC Integrate the weight curve y from x to L/2

Line 1264-1378: Subroutine WTPUT Insert weight curve points at the hydrodynamic stations
Flywheel variables added

Line 1379-1511: Subroutine NORMAL Compute the unit normals
Flywheel variables added

Line 1512-1604: Subroutine TRANS Compute blunt end unit normals

Line 1605-1618: Subroutine VECTOR Compute the vector between given points

Line 1619-1644: Subroutine XMID Find mid-points

Line 1645-1657: Subroutine CROSS Find the cross product

Line 1658-1677: Subroutine MOMTR Compute the transverse moment of inertia of the waterplane

Line 1678-1926: Subroutine PRELMC Read in and set up sea state data
Flywheel variables added

Lines 1927-2060: Subroutine SPECTR This subroutine computes ordinates of wave spectrum

Line 2061-2078: Subroutine WSTAT Compute wave statistics from spectrum

Line 2079-2107: Subroutine PERIOD Compute wave periods from spectrum

Line 2108-2125: Function TRAP Integrate area, first moment, second moment using trapezoidal rule

Line 2126-2170: Function XINT Compute an integral using the trapezoidal rule and y(x) at n points

Line 2171-2263: Subroutine TWODIM Setup calculation of sectional properties.
Flywheel variables added

Line 2264-2360: Subroutine ALINT Find interpolated values of the radiation potentials for dimensional wave number
Flywheel variables added

Line 2361-2520: Subroutine FRANK Compute the complex potential for the radiation problems
Flywheel variables added

Line 2521-2543: Subroutine FDTHWN Find the finite depth wave number

Line 2544-2574: Subroutine G2S1 Calculating the integral G(2*S+1)

Line 2575-2600: Subroutine SETUP Interpolation by piecewise cubic splines

Line 2601-2631: Subroutine SPLINE Create spline values

Line 2633-2732: Subroutine GSS Calculation of G2S1 for small KH by the corrected equations

Line 2733-2773: Subroutine MU Calculation of local wave number for finite depth

Line 2774-2786: Function ASIGN Find the sign of real(z)

Line 2787-2813: Subroutine BRANCH Account for the proper branch cut when considering two complex logs

Line 2814-2921: Subroutine WAVFRE Find the frequency independent parts of the Green's Function

Line 2922-3028: Subroutine GREEN Find the frequency dependent parts of the Green's Function

Line 3029-3089: Subroutine COEF2D Setup the coefficient matrix for the 2-D value problem
Flywheel variables added

Line 3090-3179: Subroutine GREENF Execute Green's Function

Line 3180-3248: Subroutine GREEN1 Green's Function for finite depth: Sayer's Method

Line 3249-3343: Subroutine FINDTH

Line 3344-3440: Subroutine GREEN2 Green's Function for finite depth: Rhee's Method

Line 3441-3466: Subroutine BCOND Setup the body boundary conditions

Line 3467-3495: Subroutine POTENT Find the potentials using Green's integral identity

Line 3496-3595: Subroutine OMTOUT Determine the added mass and damping coefficients for the OMT file
Flywheel variables added

Line 3596-3649: Subroutine RADFOR Find the radiation forces for the different stations
Flywheel variables added

Line 3650-3767: Complex Function CEI Determine the complex exponential integral

Line 3768-3869: Subroutine EXFORC Determine the sectional wave exciting forces
Flywheel variables added

Line 3870-3982: Subroutine ROLD Compute roll natural frequency including effects of added mass
Flywheel variables added

Line 3983-4077: Subroutine ALINTR Find interpolated values of the radiation potentials for dimensional wave number
Flywheel variables added

Line 4078-4131: Subroutine RDFOCR Find the radiation forces for the different stations
Flywheel variables added

Line 4132-4223: Subroutine COEFR Compute added mass and damping coefficients for the special case of horizontal plane motion
Flywheel variables added

Line 4224-4444: Subroutine COEFF Compute added mass and damping coefficients. The C-matrix is called on to do certain calculations in this subroutine
Flywheel variables added

Line 4445-4652: Subroutine EXCITE Compute exciting forces. CONTRL Common term
Flywheel variables added

Line 4653-4686: Subroutine FILON Compute an integral using trapezoidal rule and Filon type approach

Line 4687-4896: Subroutine RAOF Compute RAO's using iteration of roll damping. EQMO Common term
Flywheel variables added

Line 4897-4971: Subroutine MOTION Solve equations of motion. EQMO Common term
Flywheel variables added

Line 4972-5060: Subroutine PTMOT Compute the motion, velocity, acceleration, acceleration+gravity, relative motion, and relative velocity given the motions at the CG and the coordinates of a point

Line 5061-5074: Subroutine POLAR Compute the magnitude and phase of a complex number

Line 5075-5106: Subroutine WDIR Resolve the RAO's into the wave direction

Line 5107-5410: Subroutine PTREG Print out the regular wave results. Line 5198-5234 focuses on printing of the RAO's as do other sections for other degrees of freedom
Flywheel variables added

Line 5411-5458: Subroutine PTITLE Print the title for regular wave motion points

Line 5459-5539: Subroutine PTWDIR Print out the RAO's resolved in the wave direction
Flywheel variables added

Line 5540-5720: Subroutine STATI Compute and print out response spectra and statistics in long-crested irregular waves
Flywheel variables added

Line 5721-5774: Subroutine PRINT1 Print the title for irregular wave motion points

Line 5775-5915: Subroutine SPREAD Subroutine to compute and print out short-crested irregular sea statistics
Flywheel variables added

Line 5916-5932: Subroutine STATC Compute the RMS amplitude, average amplitude, significant amplitude, and the 1/10th highest amplitude given the mean square value

Line 5933-5945: Function SINT Perform trapezoidal integration of evenly spaced ordinates

Line 5946-6181: Subroutine CLUD Computes the LU-Decomposition of a matrix using Gaussian Elimination with partial pivoting

Line 6182-6221: Subroutine MESSGE Print message concerning output form

Line 6223-6325: Subroutine HIMENO Calculate the roll damping with Himeno's method
Flywheel variables added

Line 6326-6351: Subroutine LIFT Calculate the lift component

Line 6352-6378: Subroutine WAVE Calculate the wave-making component

Line 6379-6400: Subroutine FRICT Calculate the frictional component

Line 6401-6544: Subroutine EDDY Calculate the eddy-making component

Line 6545-6621: Subroutine BK Calculate damping due to bilge keels

Line 6622-6643: Subroutine HOKAN1 Do Lagrange 3-point interpolation

Line 6644-6664: Subroutine LAG3 To be used with HOKAN1

Line 6665-6701: Subroutine EDDY2 Calculate eddy-damping for a box barge with a sharp bilge

Line 6702-6712: Subroutine SEKI Integrate by Simpson's Rule for use with EDDY2

Line 6713-6770: Subroutine PRHIMO Setup roll damping parameters to be used with subroutine HIMENO
Flywheel variables added

Line 6771-6851: Subroutine BMCALM Compute the calm water shear and bending moment
Flywheel variables added

Line 6852-6916: Subroutine BENDM Compute the dynamic bending moments. EQMO Common term
Flywheel variables added

Line 6917-6981: Subroutine VNERT Compute the inertia loads of the ship mass. EQMO Common term
Flywheel variables added

Line 6982-7034: Subroutine VHSTAT Compute the hydrostatic loads. EQMO Common term
Flywheel variables added

Line 7035-7157: Subroutine VEXF Compute the exciting force loads. EQMO Common term
Flywheel variables added

Line 7158-7283: Subroutine VRADF Compute the radiation force loads. EQMO Common term
Flywheel variables added

Line 7284-7345: Subroutine TRMFIX Set constants for transom end corrections

Line 7346-7429: Subroutine PREBM Pre-compute constants used in BM calculations
Flywheel variables added

Line 7430: Real Function GMMMA Calculates the GMMA function for a real argument